What are the Kuiper Belt objects telling us about planet formation?

Wladimir Lyra

New Mexico State University

The *Planet Formation in the Southwest* Collaboration (PFITS+): Manuel Cañas (New Mexico State University)**, Daniel Carrera** (New Mexico State University), **Anders Johansen** (University of Copenhagen)**, Leonardo Krapp** (University of Arizona)**, Debanjan Sengupta** (New Mexico State University)**, Jake Simon** (Iowa State University)**, Orkan Umurhan** (NASA Ames), **Chao-Chin Yang** (University of Alabama)**, Andrew Youdin** (University of Arizona)**.**

Progress in Understanding the Pluto System - 10yrs After Flyby

APL - Laurel MD - Jul 16th, 2025

The Planetary Science Journal, 5:55 (17pp), 2024 February https://doi.org/10.3847/PSJ/ad1d5b

A Solution for the Density Dichotomy Problem of Kuiper Belt Objects with Multispecies Streaming Instability and Pebble Accretion

Manuel H. Cañas[1], Wladimir Lyra[1], Daniel Carrera[2], Leonardo Krapp[3,7], Debanjan Sengupta[1], Jacob B. Simon[2], Orkan M. Umurhan[4], Chao-Chin Yang (楊朝欽)[5], and Andrew N. Youdin[3,6]
[1] New Mexico State University, Department of Astronomy, P.O. Box 30001 MSC 4500, Las Cruces, NM 88001, USA; wlyra@nmsu.edu
[2] Department of Physics and Astronomy, Iowa State University, Ames, IA 50010, USA
[3] Department of Astronomy and Steward Observatory, University of Arizona, Tucson, AZ 85721, USA
[4] NASA Ames Research Center, Space Sciences Division, Planetary Sciences Branch, Moffatt Field, CA 94035, USA
[5] Department of Physics and Astronomy, University of Alabama, Box 870324, Tuscaloosa, AL 35487-0324, USA
[6] The Lunar and Planetary Laboratory, University of Arizona, Tucson, AZ 85721, USA
Received 2023 August 25; revised 2023 December 27; accepted 2024 January 5; published 2024 February 28

Abstract

Kuiper Belt objects (KBOs) show an unexpected trend, whereby large bodies have increasingly higher densities, up to five times greater than their smaller counterparts. Current explanations for this trend assume formation at constant composition, with the increasing density resulting from gravitational compaction. However, this scenario poses a timing problem to avoid early melting by decay of ^{26}Al. We aim to explain the density trend in the context of streaming instability and pebble accretion. Small pebbles experience lofting into the atmosphere of the disk, being exposed to UV and partially losing their ice via desorption. Conversely, larger pebbles are shielded and remain icier. We use a shearing box model including gas and solids, the latter split into ices and silicate pebbles. Self-gravity is included, allowing dense clumps to collapse into planetesimals. We find that the streaming instability leads to the formation of mostly icy planetesimals, albeit with an unexpected trend that the lighter ones are more silicate-rich than the heavier ones. We feed the resulting planetesimals into a pebble accretion integrator with a continuous size distribution, finding that they undergo drastic changes in composition as they preferentially accrete silicate pebbles. The density and masses of large KBOs are best reproduced if they form between 15 and 22 au. Our solution avoids the timing problem because the first planetesimals are primarily icy and ^{26}Al is mostly incorporated in the slow phase of silicate pebble accretion. Our results lend further credibility to the streaming instability and pebble accretion as formation and growth mechanisms.

Unified Astronomy Thesaurus concepts: Dwarf planets (419); Kuiper Belt (893); Pluto (1267); Hydrodynamics (1963); Planet formation (1241)

The Astrophysical Journal, 946:60 (14pp), 2023 April 1 https://doi.org/10.3847/1538-4357/acaf5b

An Analytical Theory for the Growth from Planetesimals to Planets by Polydisperse Pebble Accretion

Wladimir Lyra[1], Anders Johansen[2,3], Manuel H. Cañas[1], and Chao-Chin Yang (楊朝欽)[4]
[1] New Mexico State University, Department of Astronomy, PO Box 30001 MSC 4500, Las Cruces, NM 88001, USA; wlyra@nmsu.edu
[2] Center for Star and Planet Formation, GLOBE Institute, University of Copenhagen, Øster Voldgade 5–7, D-1350 Copenhagen, Denmark
[3] Lund Observatory, Department of Astronomy and Theoretical Physics, Lund University, Box 43, SE-221 00 Lund, Sweden
[4] Department of Physics and Astronomy, University of Alabama, Box 870324, Tuscaloosa, AL 35487-0324, USA
Received 2022 September 6; revised 2022 December 19; accepted 2022 December 29; published 2023 March 30

Abstract

Pebble accretion is recognized as a significant accelerator of planet formation. Yet only formulae for single-sized (monodisperse) distribution have been derived in the literature. These can lead to significant underestimates for Bondi accretion, for which the best accreted pebble size may not be the one that dominates the mass distribution. We derive in this paper the polydisperse theory of pebble accretion. We consider a power-law distribution in pebble radius, and we find the resulting surface and volume number density distribution functions. We derive also the exact monodisperse analytical pebble accretion rate for which 3D accretion and 2D accretion are limits. In addition, we find analytical solutions to the polydisperse 2D Hill and 3D Bondi limits. We integrate the polydisperse pebble accretion numerically for the MRN distribution, finding a slight decrease (by an exact factor 3/7) in the Hill regime compared to the monodisperse case. In contrast, in the Bondi regime, we find accretion rates 1–2 orders of magnitude higher compared to monodisperse, also extending the onset of pebble accretion to 1–2 orders of magnitude lower in mass. We find megayear timescales, within the disk lifetime, for Bondi accretion on top of planetary seeds of masses 10^{-6} to 10^{-4} $M_\oplus$, over a significant range of the parameter space. This mass range overlaps with the high-mass end of the planetesimal initial mass function, and thus pebble accretion is possible directly following formation by streaming instability. This alleviates the need for mutual planetesimal collisions as a major contribution to planetary growth.

Unified Astronomy Thesaurus concepts: Planet formation (1241); Planetary system formation (1257)

Where are the missing Kuiper Belt binaries?

Wladimir Lyra[a,*]
[a] *New Mexico State University, Department of Astronomy, PO Box 30001 MSC 4500, Las Cruces, 88001, NM, USA*

ARTICLE INFO

Keywords:
Kuiper belt
Planetesimals
Binaries
Origin, solar system
Planetary formation

ABSTRACT

In this letter, we call attention to a gap in binaries in the Kuiper belt in the mass range between 10^{-3} and 10^{-2} Pluto masses ($\approx 10^{19}$-10^{20} kg), with a corresponding dearth in binaries between 4th and 5th absolute magnitude H. The low-mass end of the gap is consistent with the truncation of the cold classical population at 400 km, as suggested by the OSSOS survey, and predicted by simulations of planetesimal formation by streaming instability. The distribution of magnitudes for all KBOs is continuous, which means that many objects exist in the gap, but the binaries in this range have either been disrupted, or the companions are too close to the primary and/or too dim to be detected with the current generation of observational instruments. At the high-mass side of the gap, the objects have small satellites at small separations, and we find a trend that as mass decreases, the ratio of primary radius to secondary semimajor increases. If this trend continues into the gap, non-Keplerian effects should make mass determination more challenging.

Icarus 356 (2021) 113831

ELSEVIER
Contents lists available at ScienceDirect
Icarus
journal homepage: www.elsevier.com/locate/icarus
ICARUS

Evolution of MU69 from a binary planetesimal into contact by Kozai-Lidov oscillations and nebular drag

Check for updates

W. Lyra[a,*], A.N. Youdin[b], A. Johansen[c]
[a] *Department of Astronomy, New Mexico State University, PO BOX 30001, MSC 4500, Las Cruces, NM 88003-8001, United States of America*
[b] *Steward Observatory, University of Arizona, Tucson, AZ 85721, United States of America*
[c] *Lund Observatory, Department of Astronomy and Theoretical Physics, Lund University, Box 43, 221 00 Lund, Sweden*

ARTICLE INFO

Keywords:
Kuiper belt
Planetesimals
Origin, solar system
Planetary formation

ABSTRACT

The New Horizons flyby of the cold classical Kuiper Belt object MU69 showed it to be a contact binary. The existence of other contact binaries in the 1–10 km range raises the question of how common these bodies are and how they evolved into contact. Here we consider that the pre-contact lobes of MU69 formed as a binary embedded in the Solar nebula, and calculate its subsequent orbital evolution in the presence of gas drag. We find that the sub-Keplerian wind of the disk brings the drag timescales for 10 km bodies to under 1 Myr for quadratic-velocity drag, which is valid in the asteroid belt. In the Kuiper belt, however, the drag is linear with velocity and the effect of the wind cancels out as the angular momentum gained in half an orbit is exactly lost in the other half; the drag timescales for 10 km bodies remain $\gtrsim$10 Myr. In this situation we find that a combination of nebular drag and Kozai-Lidov oscillations is a promising channel for collapse. We analytically solve the hierarchical three-body problem with nebular drag and implement it into a Kozai cycles plus tidal friction model. The permanent quadrupoles of the pre-merger lobes make the Kozai oscillations stochastic, and we find that when gas drag is included the shrinking of the semimajor axis more easily allows the stochastic fluctuations to bring the system into contact. Evolution to contact happens very rapidly (within 10^4 yr) in the pure, double-average quadrupole, Kozai region between $\approx 85 - 95^\circ$, and within 3 Myr in the drag-assisted region beyond it. The synergy between J_2 and gas drag widens the window of contact to $80^\circ - 100^\circ$ initial inclination, over a larger range of semimajor axes than Kozai and J_2 alone. As such, the model predicts a low initial occurrence of binaries in the asteroid belt, and an initial contact binary fraction of about 10% for the cold classicals in the Kuiper belt. The speed at contact is the orbital velocity; if contact happens at pericenter at high eccentricity, it deviates from the escape velocity only because of the oblateness, independently of the semimajor axis. For MU69, the oblateness leads to a 30% decrease in contact velocity with respect to the escape velocity, the latter scaling with the square root of the density. For mean densities in the range 0.3–0.5 g cm^{-3}, the contact velocity should be 3.3 – 4.2 m s^{-1}, in line with the observational evidence from the lack of deformation features and estimate of the tensile strength.

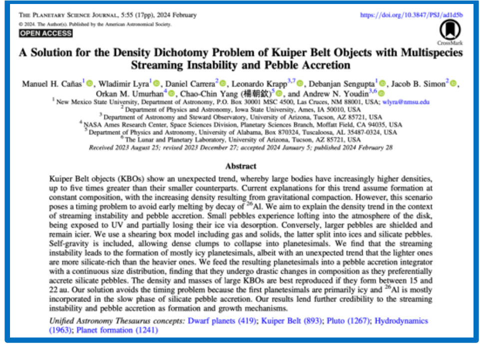

THE PLANETARY SCIENCE JOURNAL, 5:55 (17pp), 2024 February https://doi.org/10.3847/PSJ/ad1d5b

A Solution for the Density Dichotomy Problem of Kuiper Belt Objects with Multispecies Streaming Instability and Pebble Accretion

Manuel H. Cañas[1], Wladimir Lyra[1], Daniel Carrera[2], Leonardo Krapp[3,7], Debanjan Sengupta[1], Jacob B. Simon[2], Orkan M. Umurhan[4], Chao-Chin Yang (楊朝欽)[5], and Andrew N. Youdin[3,6]
[1] New Mexico State University, Department of Astronomy, P.O. Box 30001 MSC 4500, Las Cruces, NM 88001, USA; wlyra@nmsu.edu
[2] Department of Physics and Astronomy, Iowa State University, Ames, IA 50010, USA
[3] Department of Astronomy and Steward Observatory, University of Arizona, Tucson, AZ 85721, USA
[4] NASA Ames Research Center, Space Sciences Division, Planetary Sciences Branch, Moffatt Field, CA 94035, USA
[5] Department of Physics and Astronomy, University of Alabama, Box 870324, Tuscaloosa, AL 35487-0324, USA
[6] The Lunar and Planetary Laboratory, University of Arizona, Tucson, AZ 85721, USA
Received 2023 August 25; revised 2023 December 27; accepted 2024 January 5; published 2024 February 28

Abstract

Kuiper Belt objects (KBOs) show an unexpected trend, whereby large bodies have increasingly higher densities, up to five times greater than their smaller counterparts. Current explanations for this trend assume formation at constant composition, with the increasing density resulting from gravitational compaction. However, this scenario poses a timing problem to avoid early melting by decay of ^{26}Al. We aim to explain the density trend in the context of streaming instability and pebble accretion. Small pebbles experience lofting into the atmosphere of the disk, being exposed to UV and partially losing their ice via desorption. Conversely, larger pebbles are shielded and remain icier. We use a shearing box model including gas and solids, the latter split into ices and silicate pebbles. Self-gravity is included, allowing dense clumps to collapse into planetesimals. We find that the streaming instability leads to the formation of mostly icy planetesimals, albeit with an unexpected trend that the lighter ones are more silicate-rich than the heavier ones. We feed the resulting planetesimals into a pebble accretion integrator with a continuous size distribution, finding that they undergo drastic changes in composition as they preferentially accrete silicate pebbles. The density and masses of large KBOs are best reproduced if they form between 15 and 22 au. Our solution avoids the timing problem because the first planetesimals are primarily icy and ^{26}Al is mostly incorporated in the slow phase of silicate pebble accretion. Our results lend further credibility to the streaming instability and pebble accretion as formation and growth mechanisms.

Unified Astronomy Thesaurus concepts: Dwarf planets (419); Kuiper Belt (893); Pluto (1267); Hydrodynamics (1963); Planet formation (1241)

The size-density relationship of Kuiper Belt objects

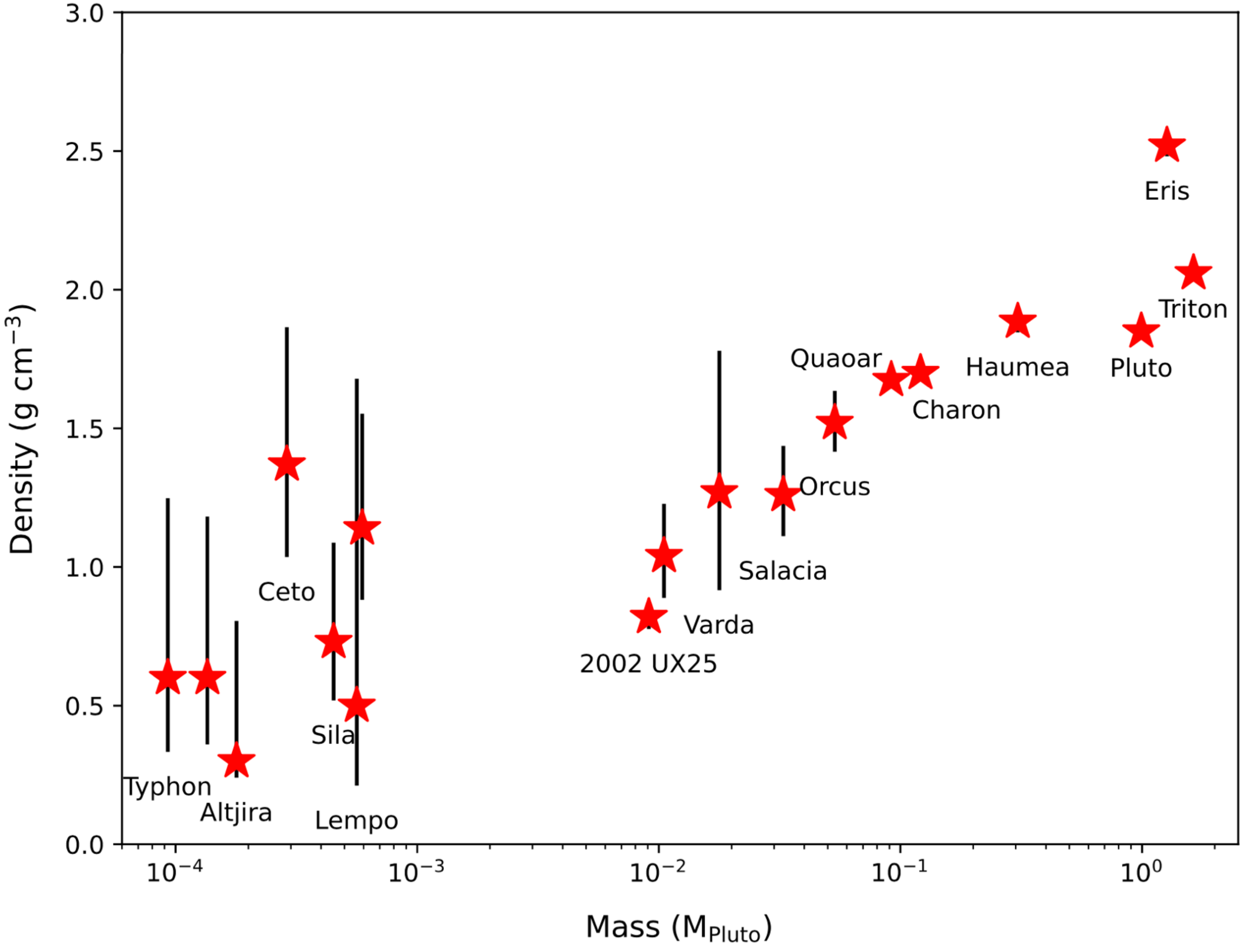

Cañas+Lyra et al. (2024)

Data; *Thomas (2000), Stansberry et al. (2006), Grundy et al. (2007), Brown et al. (2011), Stansberry et al. (2012), Brown (2013), Fornasier et al. (2013), Vilenius, et al. (2014), Nimmo et al. (2016), Ortiz et al. (2017), Brown and Butler (2017), Grundy et al. (2019), Morgado et al. (2023), Pereira et al. (2023).*

Previous best bet:
Porosity removal by gravitational compaction

Problem

- Timing! ^{26}Al would melt if formed within 4 Myr

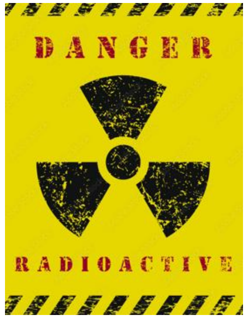

Assumptions

- ~~Constant composition at birth and growth~~
- ~~Growth by planetesimal accretion~~

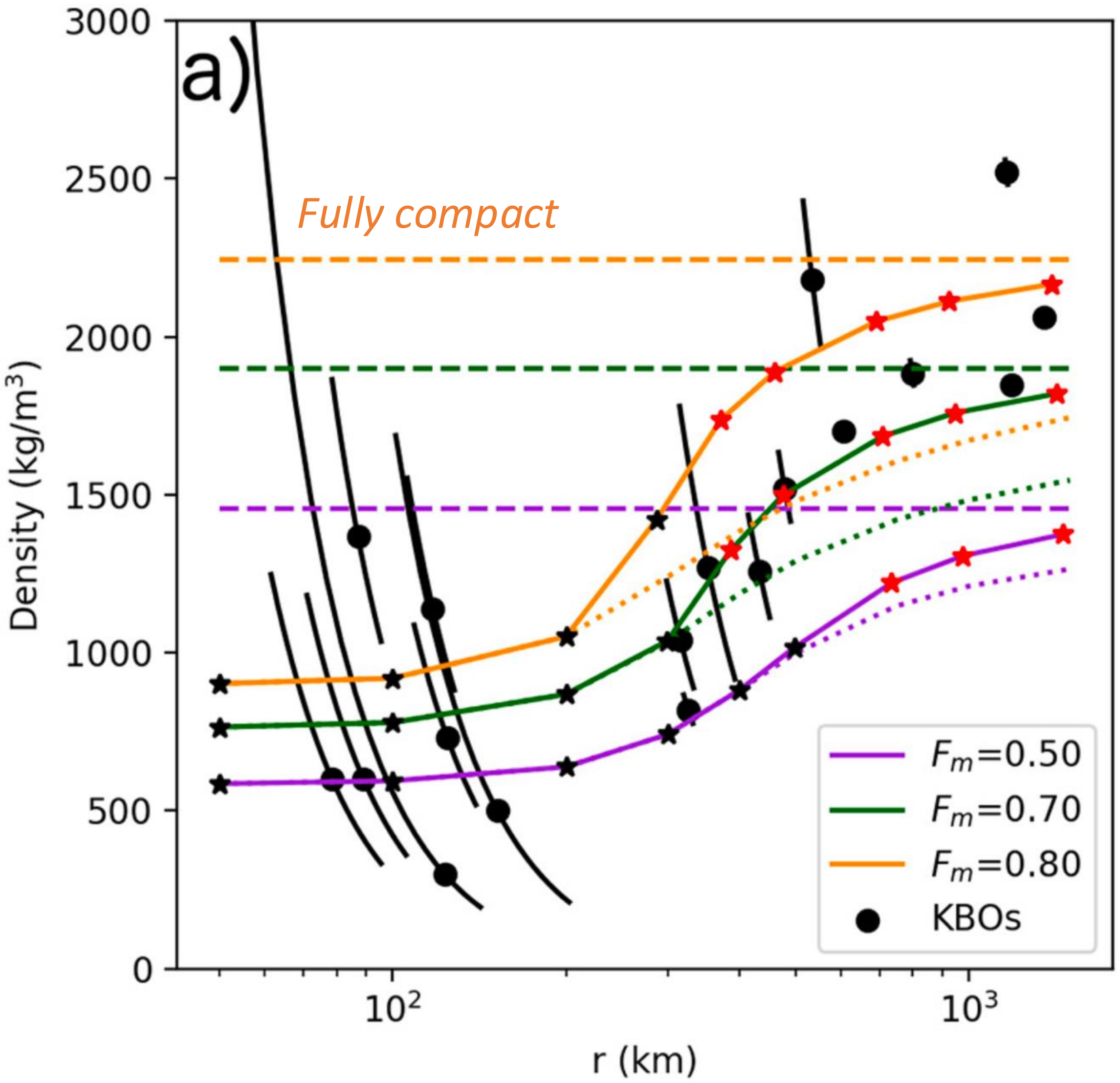

F_m = rock mass fraction

Bierson & Nimmo (2019)

Streaming Instability

The dust drift is hydrodynamically unstable

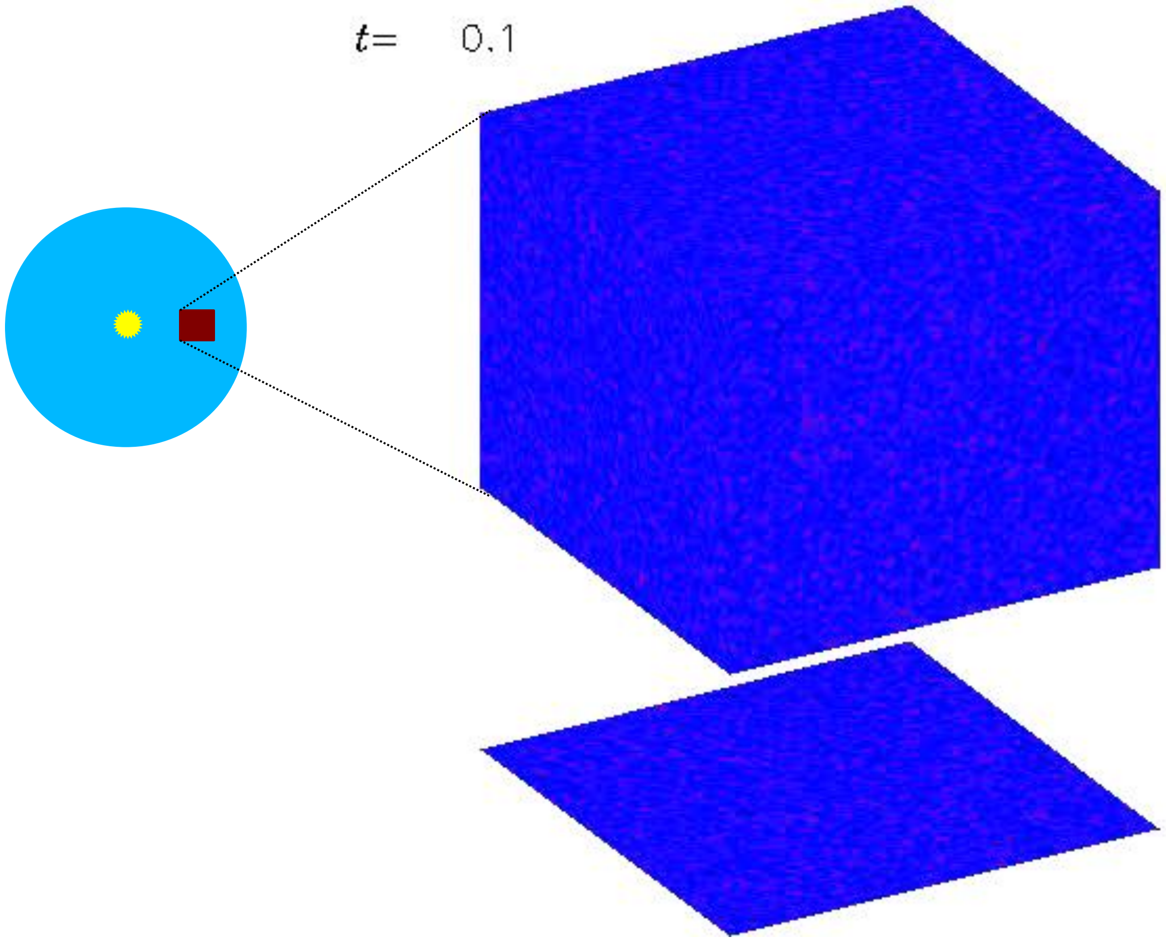

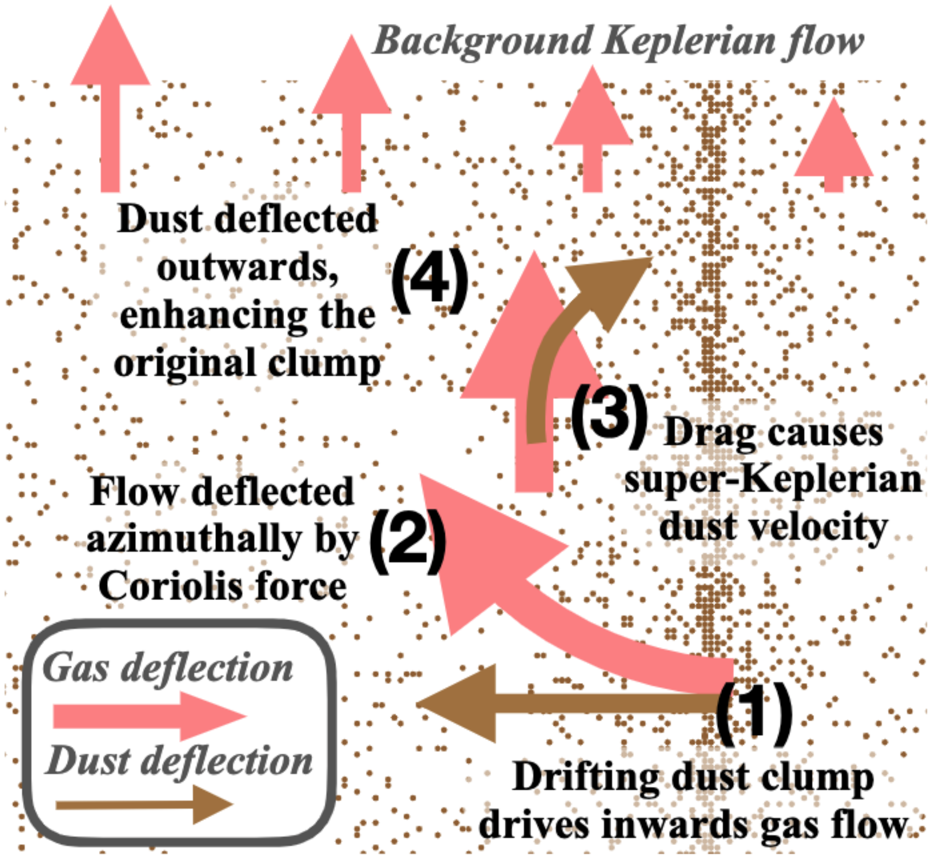

Lesur et al. (2022)

Youdin & Goodman ‘05, Johansen & Youdin ‘07, Youdin & Johansen+ ‘07, Kowalik+ ’13, Lyra & Kuchner ‘13,
Schreiber+ ‘18, Klahr & Schreiber ’20, Simon+ ‘16, ‘17, Carrera+ ‘15, ‘17, ‘20, Gole+ ’20, Li+ ‘18, ‘19, Abod+ ’19, Nesvorny+ ’19

Abandoning Constant Composition

Heating and UV irradiation remove ice on Myr timescales (Harrison & Schoen 1967)

- Small grains lofted in the atmosphere lose ice
- Big grains are shielded and remain icy.

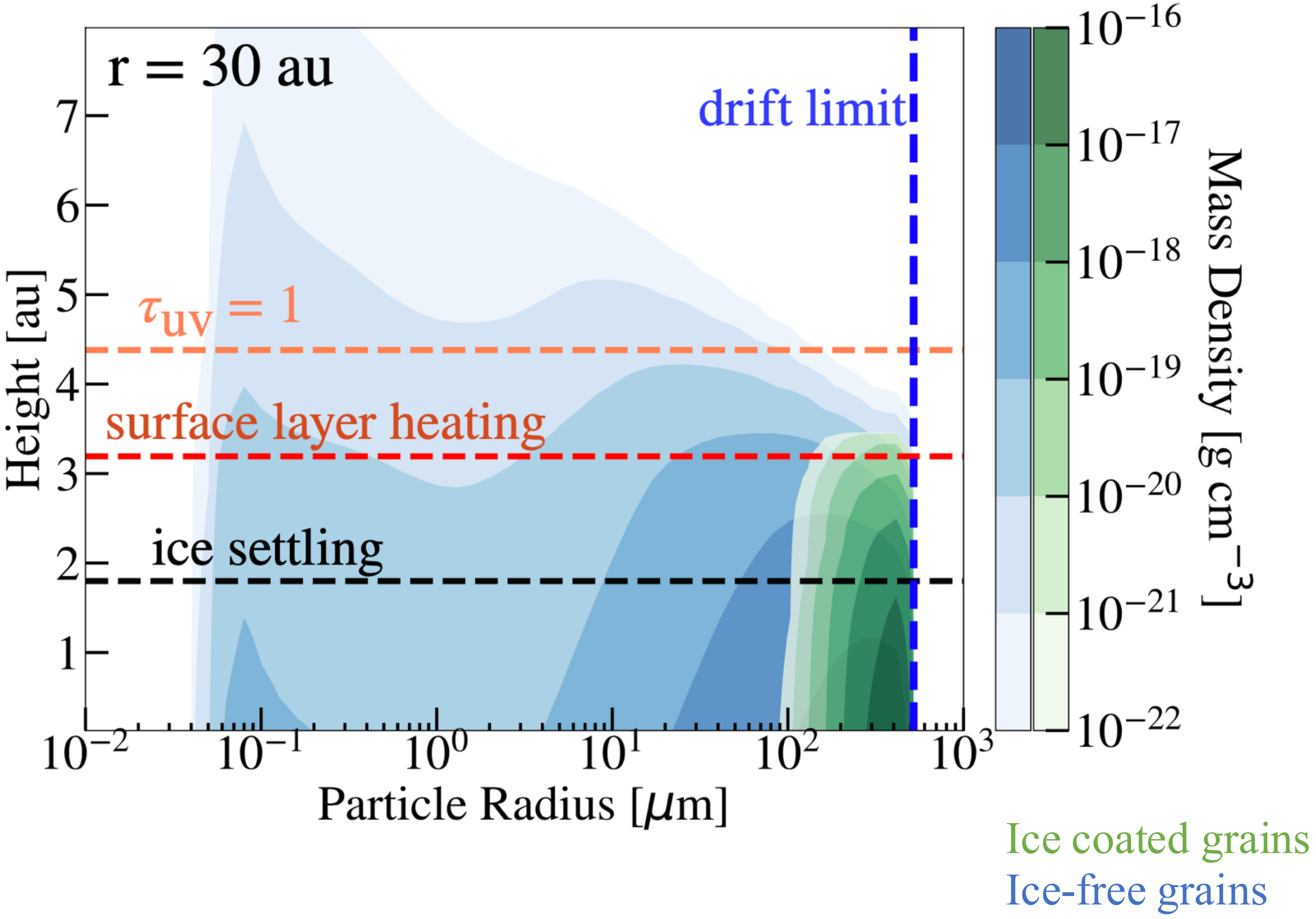

Powell et al. 2022

Split into icy and silicate pebbles

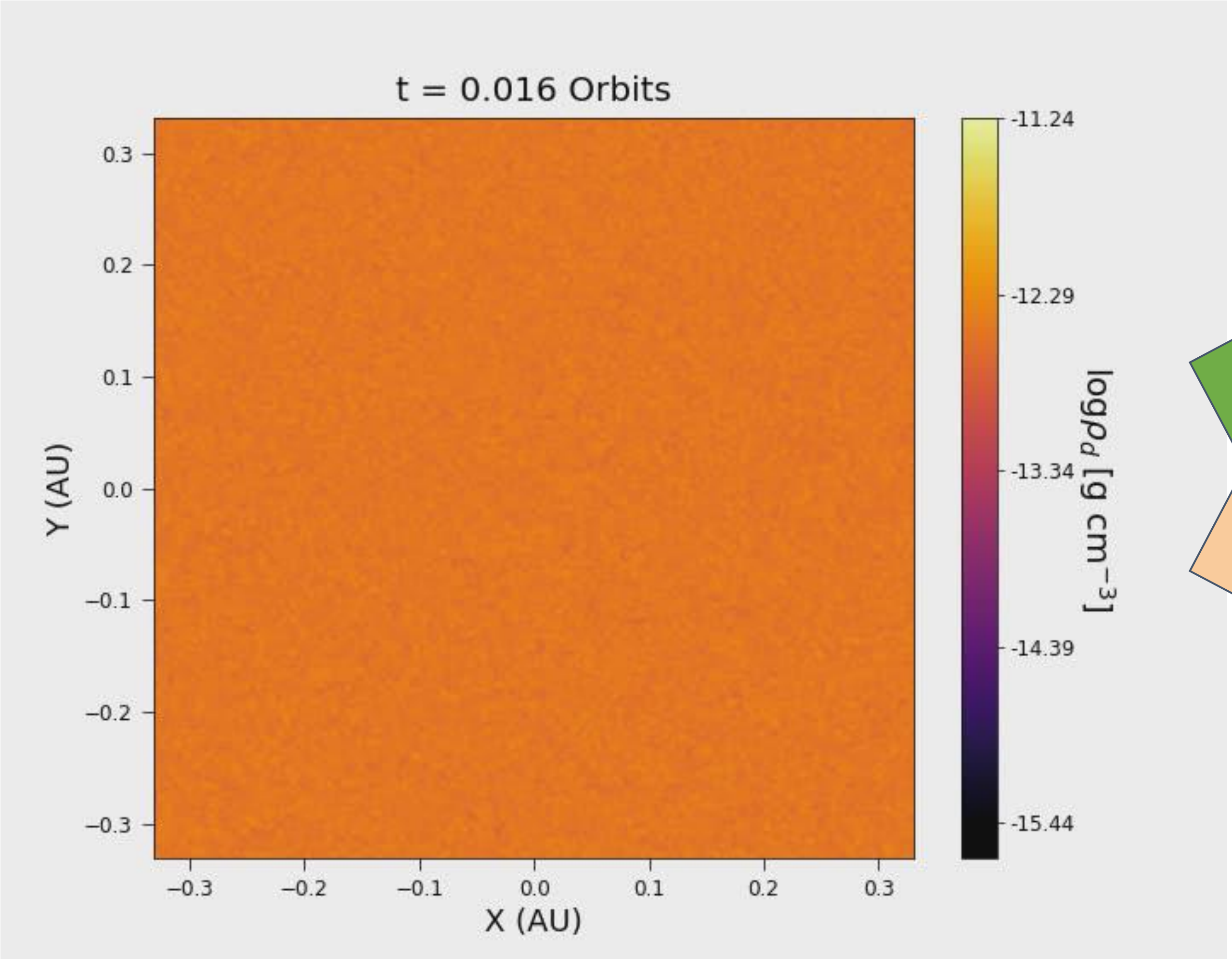

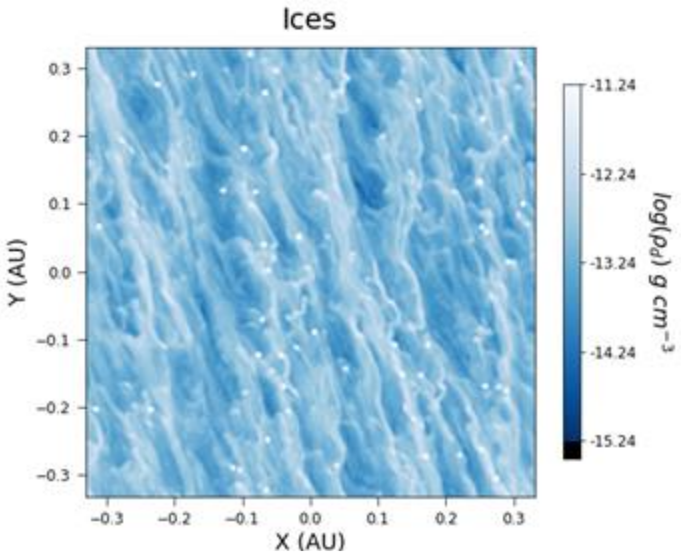

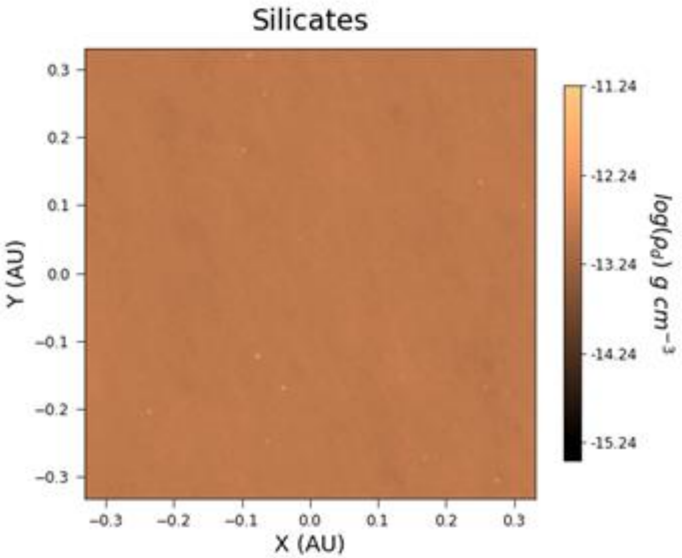

Canas+Lyra et al. 2024

The first planetesimals are icy

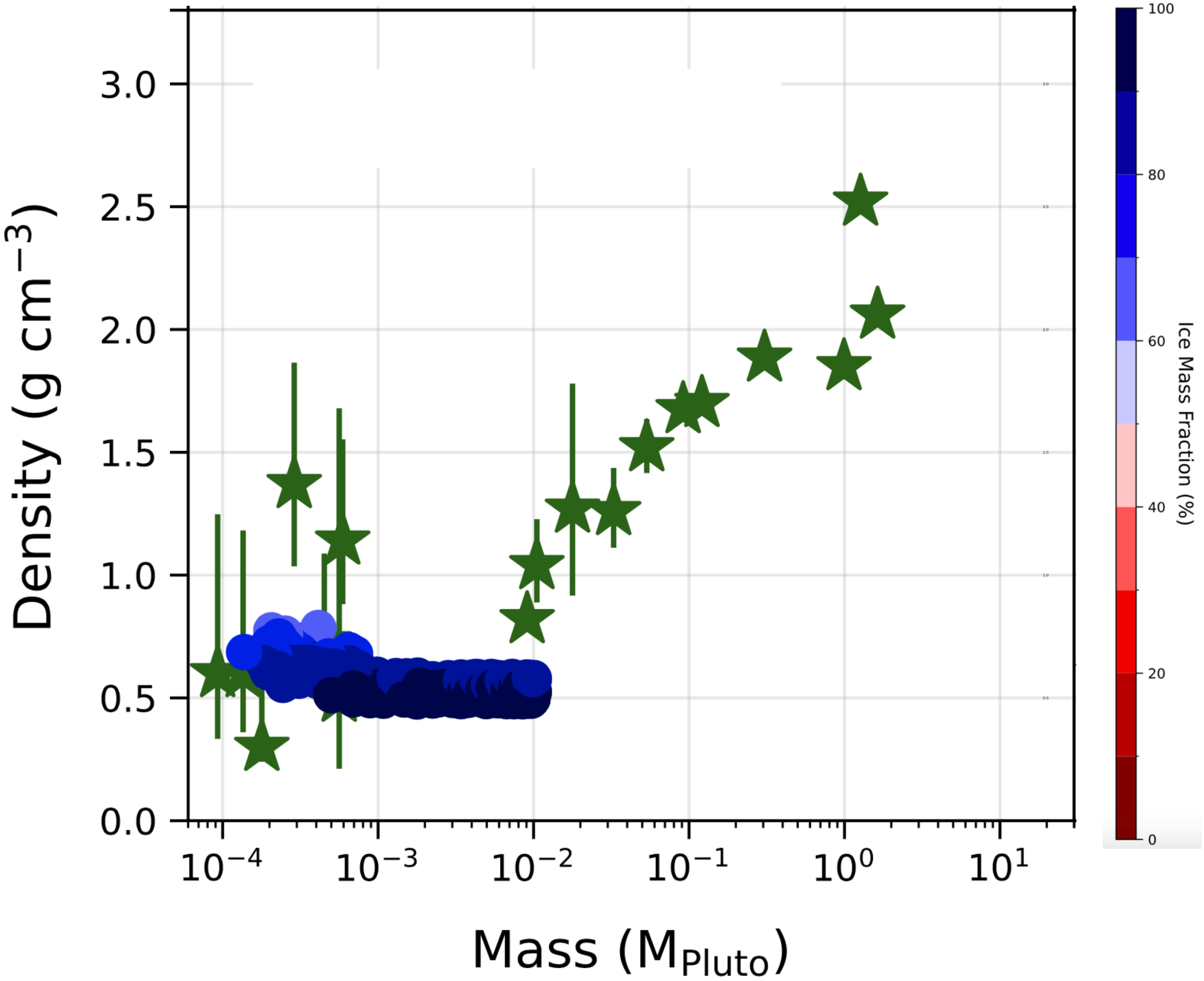

Canas+Lyra et al. 2024

Core Accretion

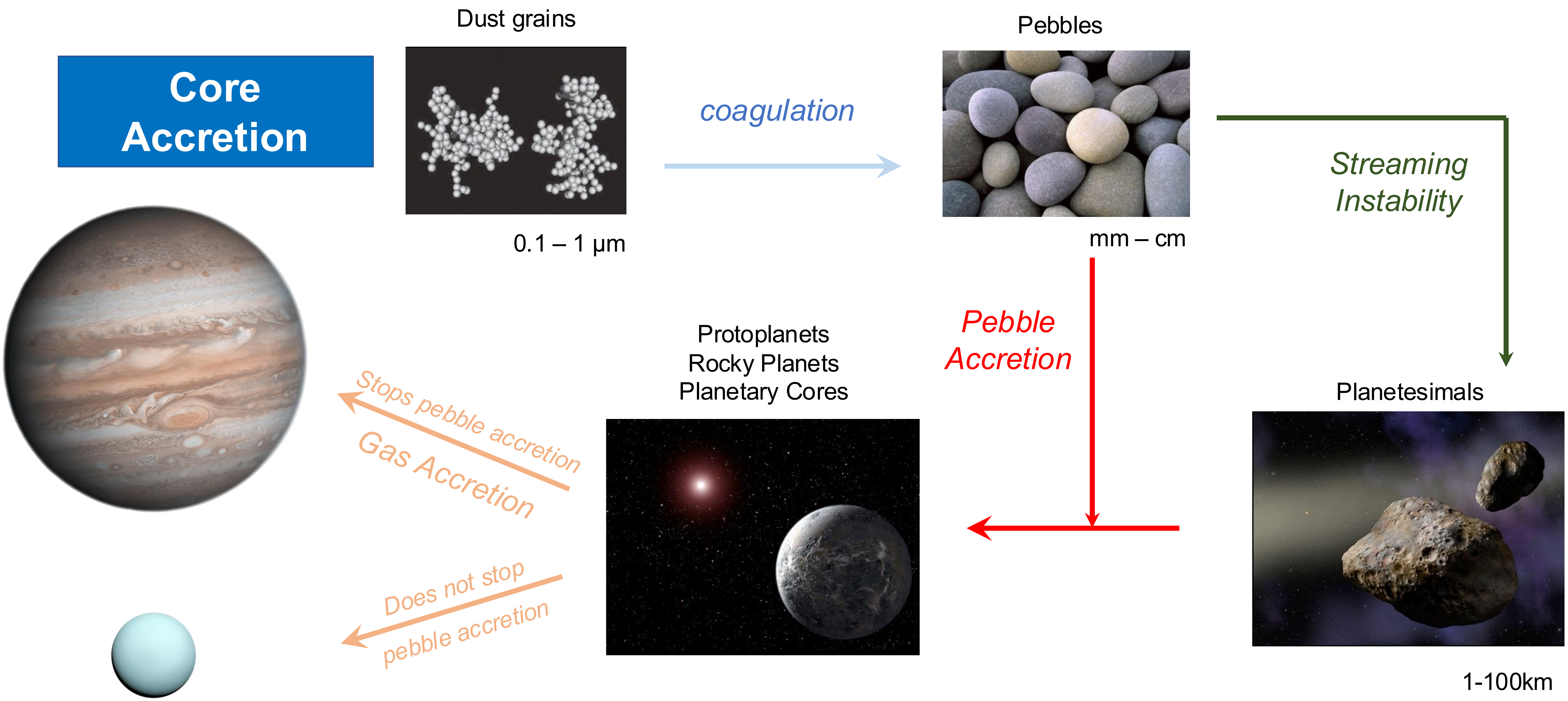

Pebble Accretion

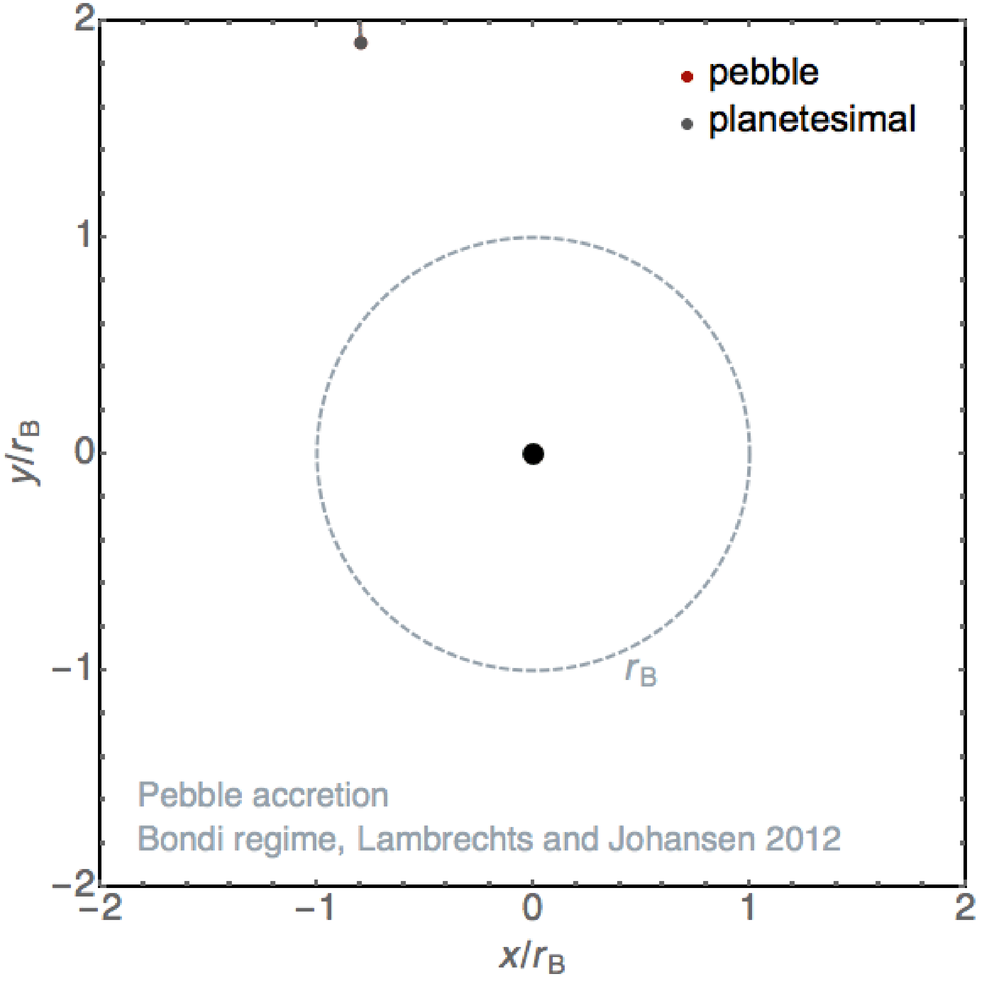

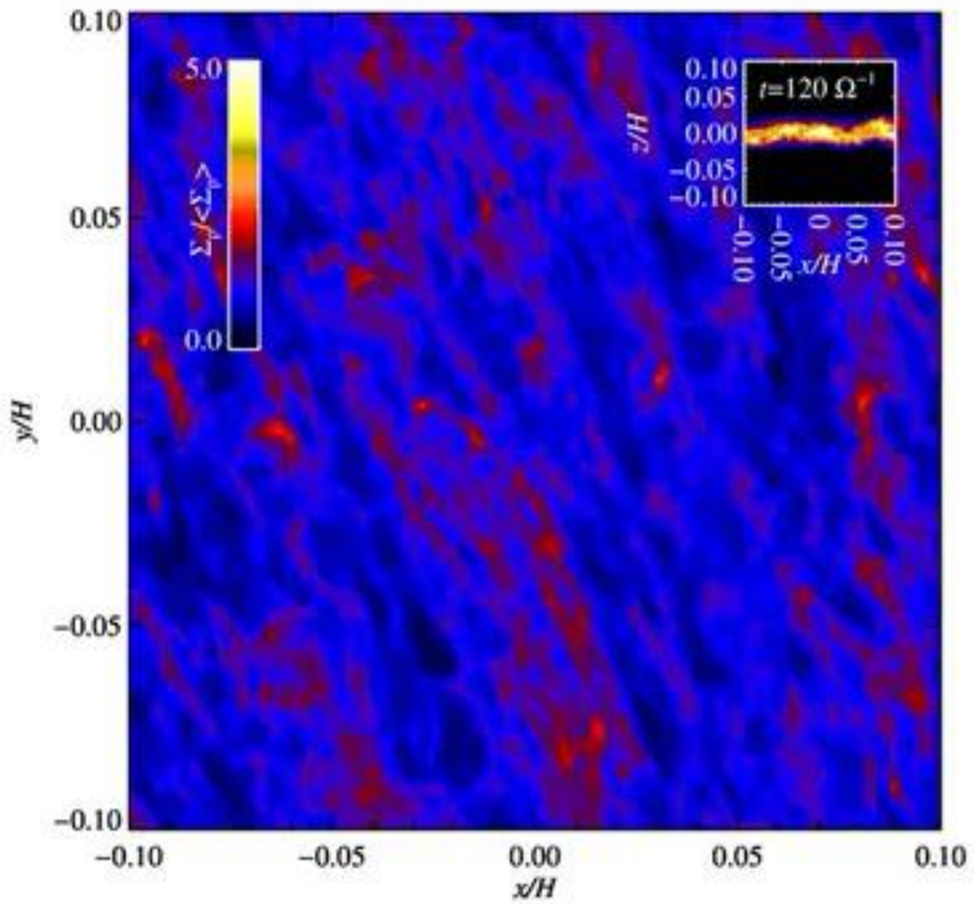

Lyra+ ‘08, ’09, ’23, Ormel & Klahr ‘10, Lambrechts & Johansen ’12
See Johansen & Lambrechts ‘17 for a review

Pebble Accretion: Geometric, Bondi, and Hill regime

Bondi accretion - Bound against headwind
Hill accretion - Bound against stellar tide

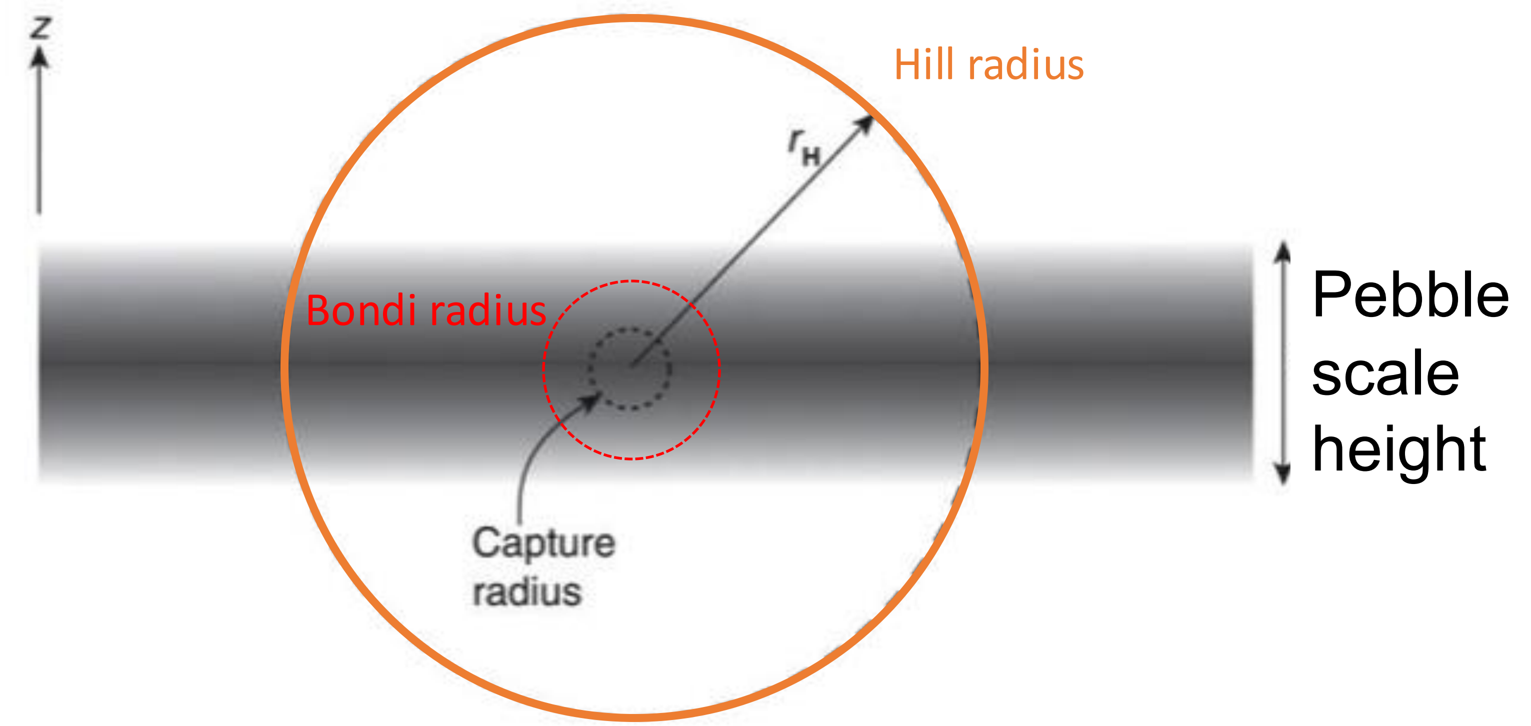

Mass Accretion rates

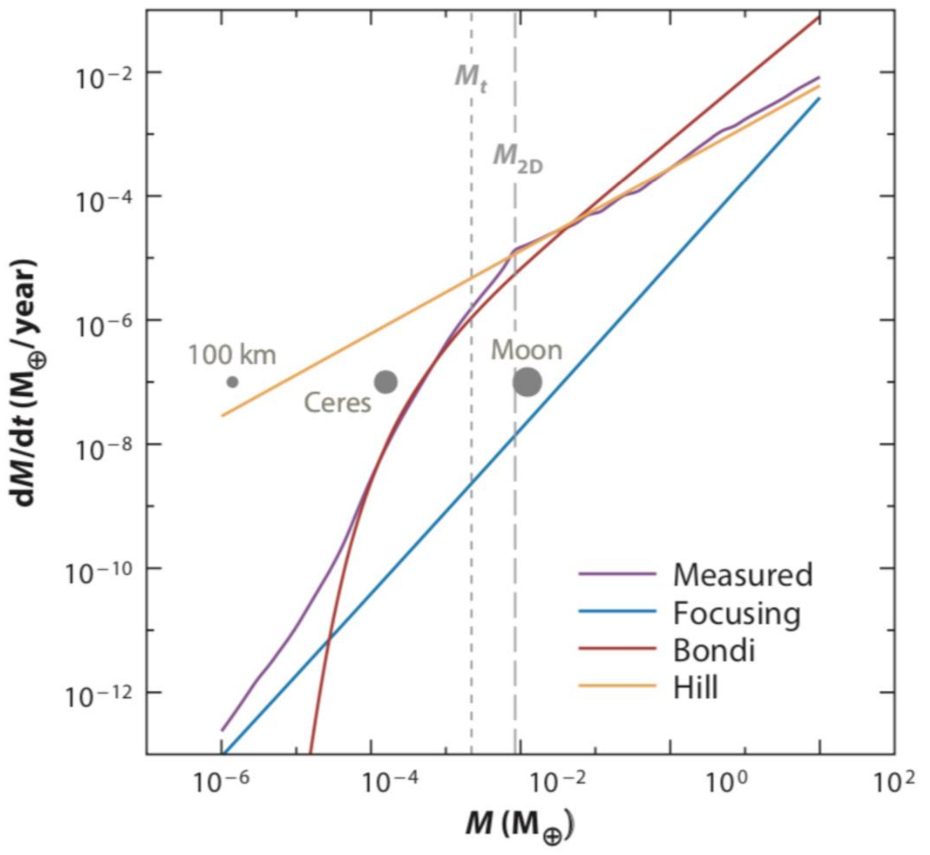

Johansen & Lambrechts (2017); Lyra et al (2023)

Integrate pebble accretion

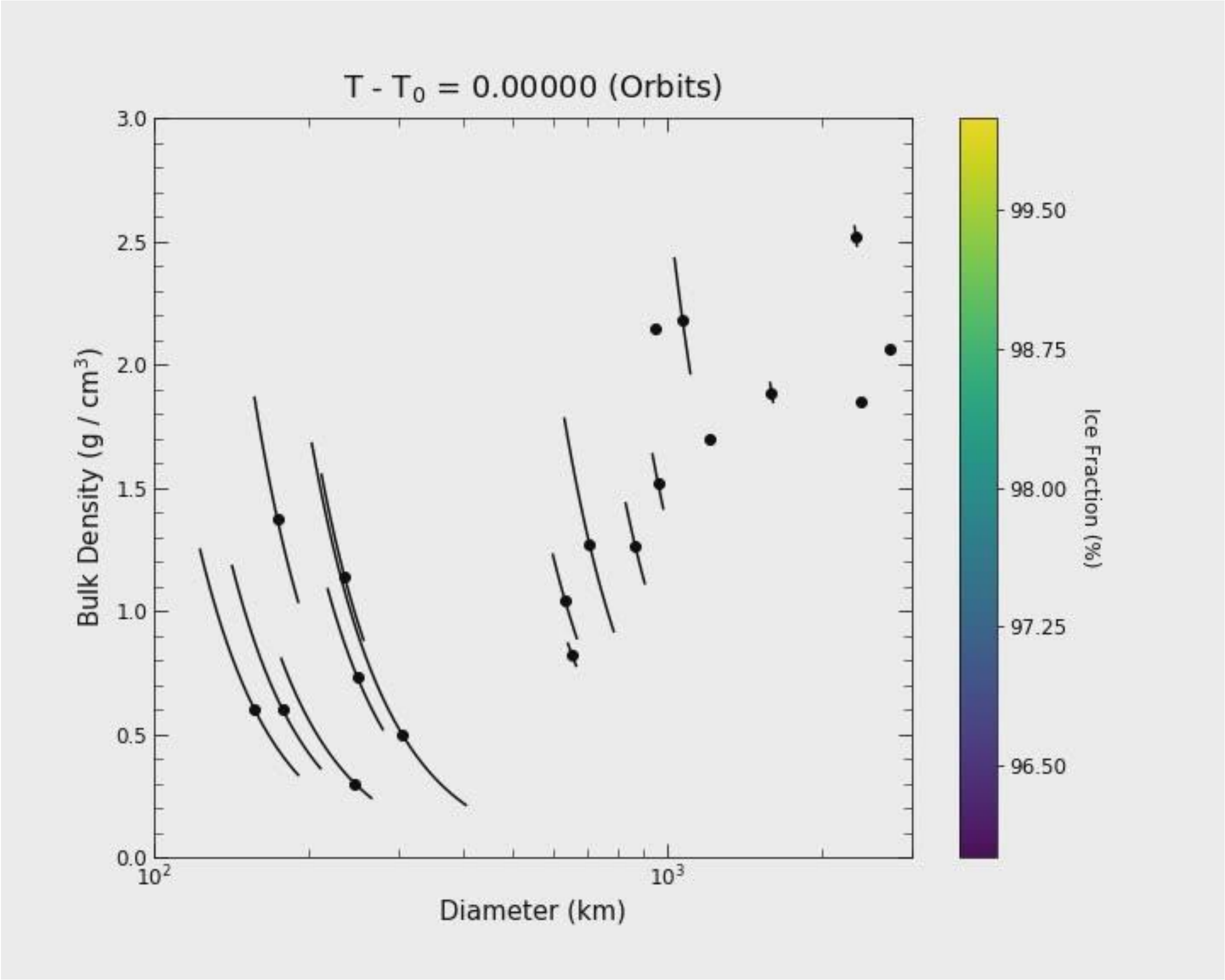

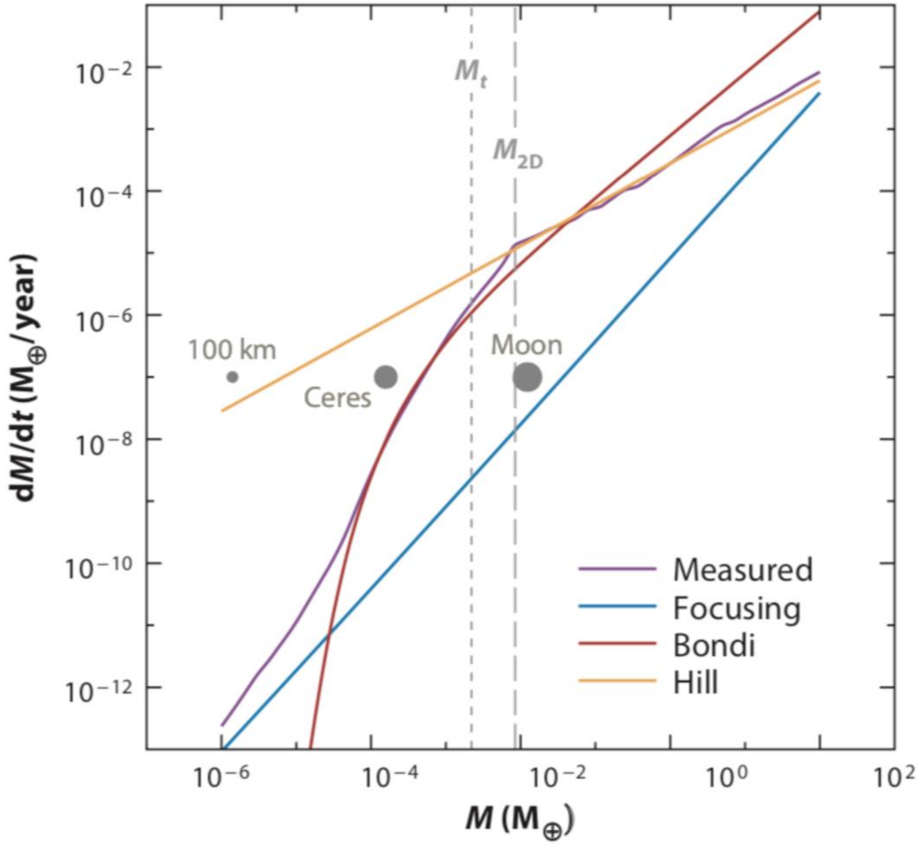

Pebble Accretion: Pebbles of different size accrete differently

”Goldilocks effect” in the Bondi regime

Large
Medium
Small

Bondi Regime

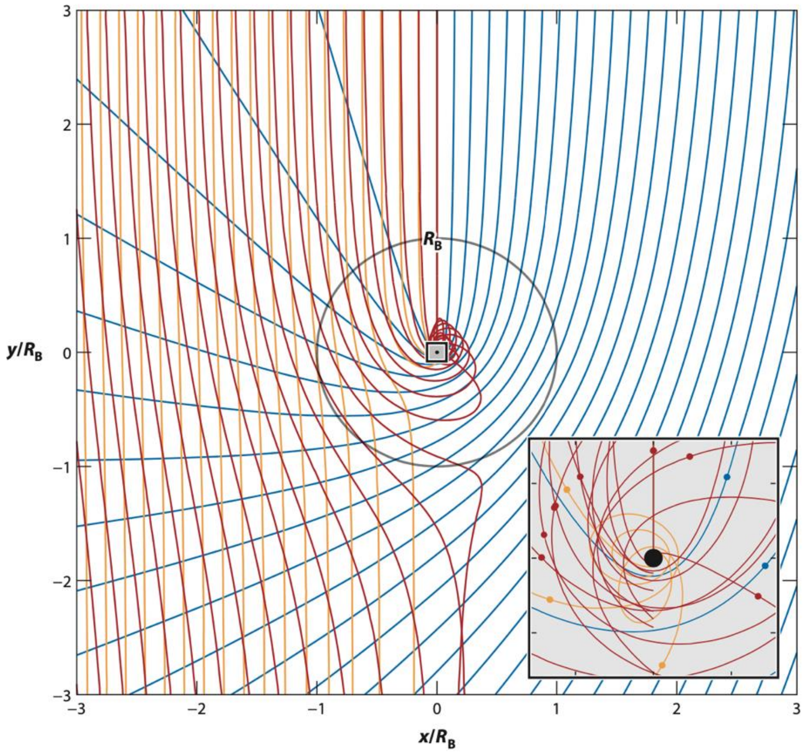

Best accreted pebble

Drag time ~ Bondi Time

Hill Regime

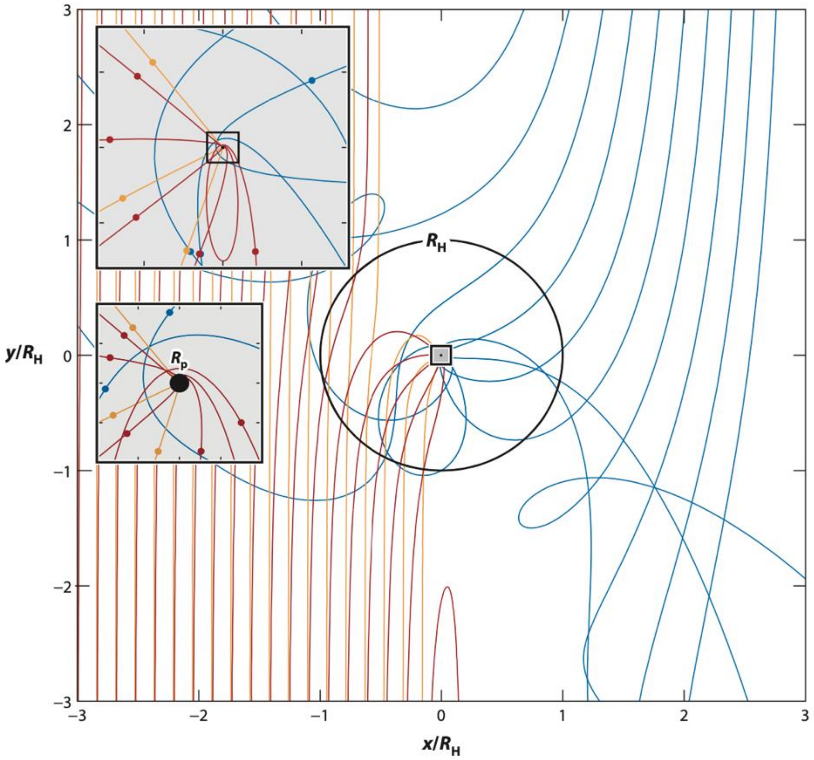

Best accreted pebble

Drag time ~ Orbital Time

Johansen & Lambrechts (2017); Lyra et al (2023)

Accretion Rates at 40 AU

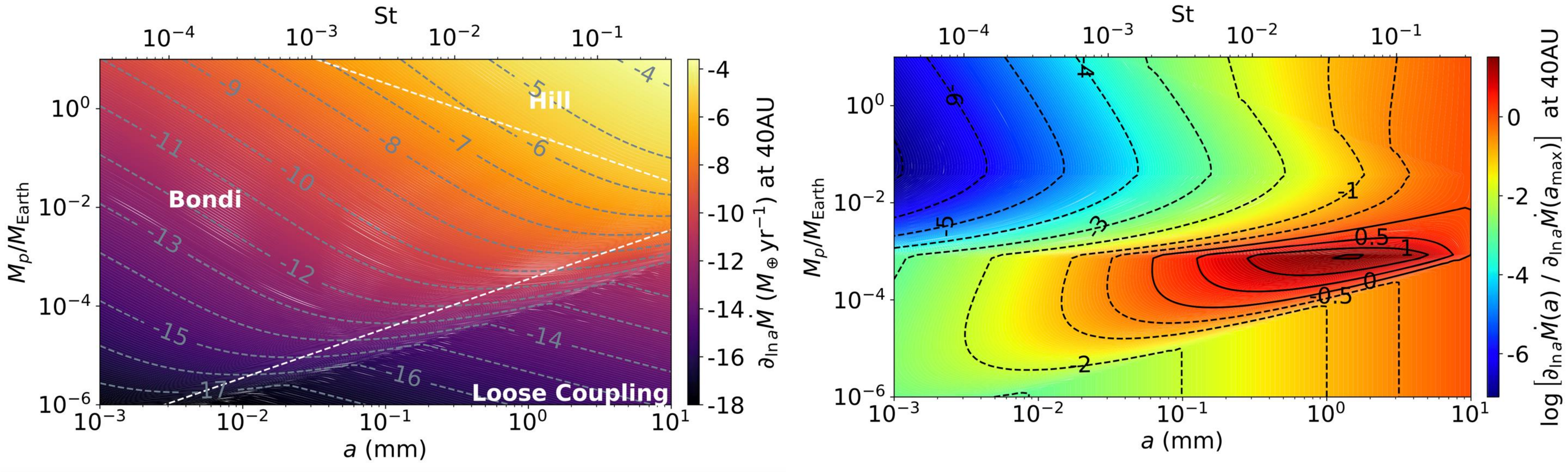

Lyra et al. 2023

Accretion Rates

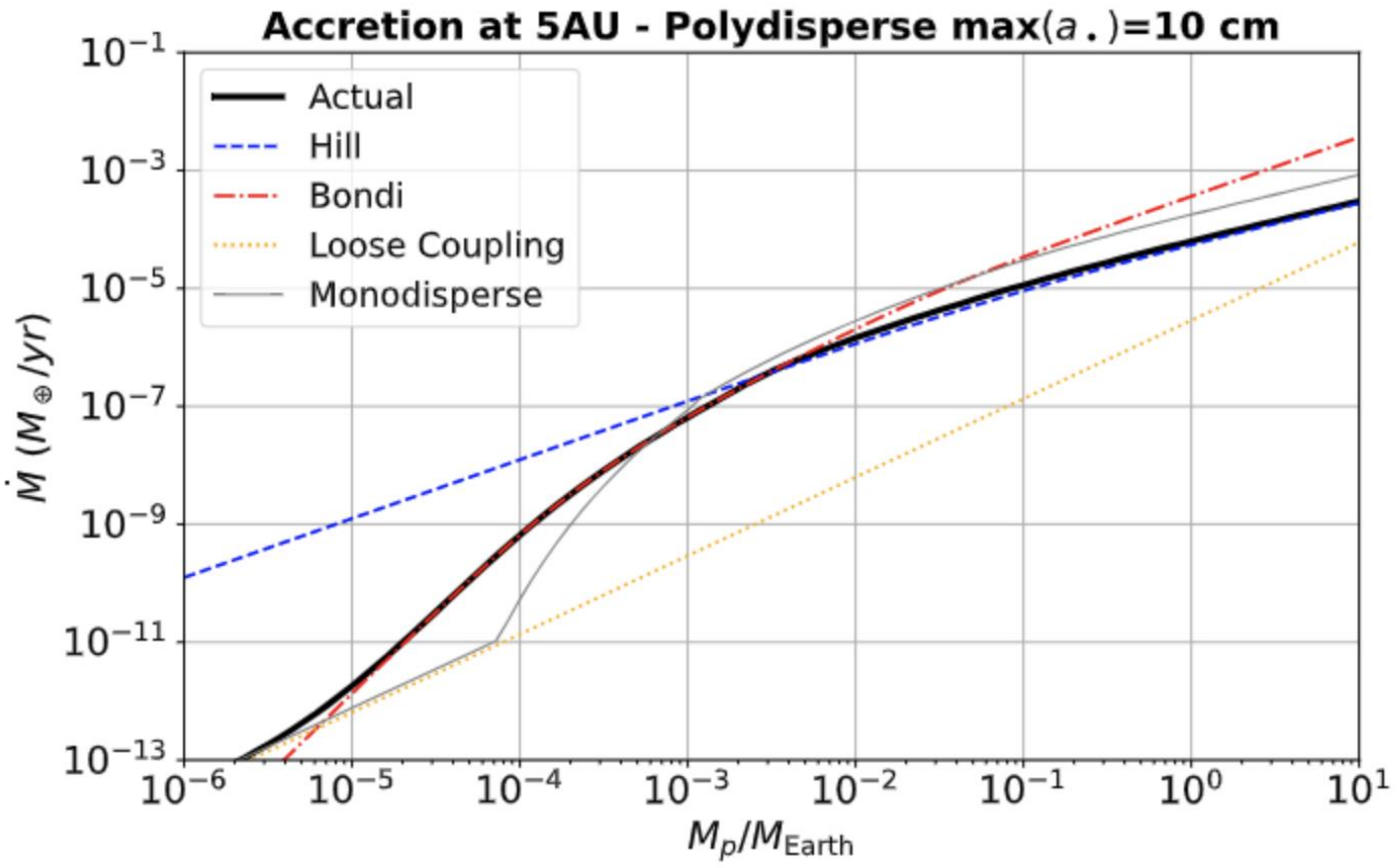

Lyra et al. 2023

Growing Pluto by silicate pebble accretion

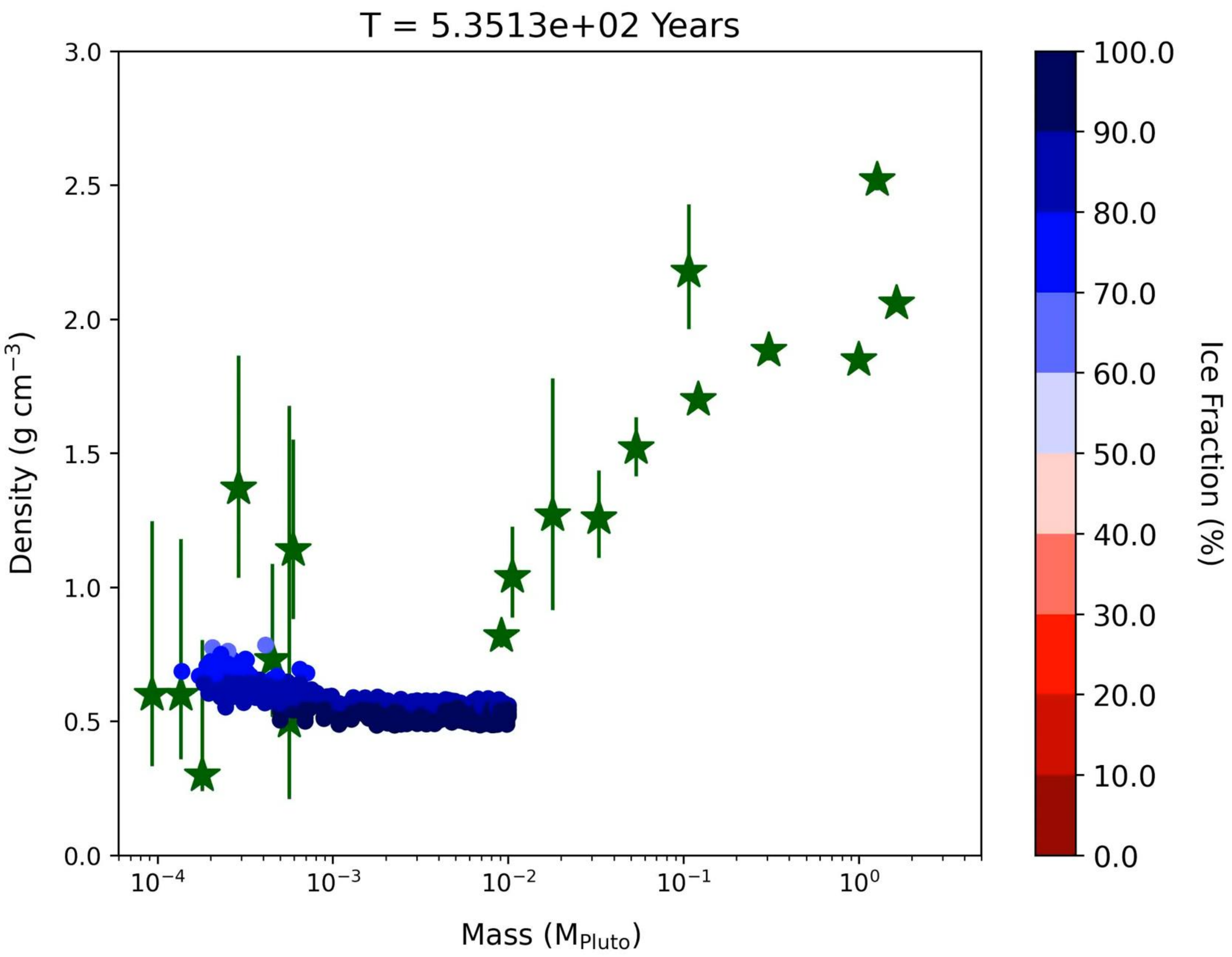

Canas+Lyra et al. 2024

Resulting Densities vs Mass relations

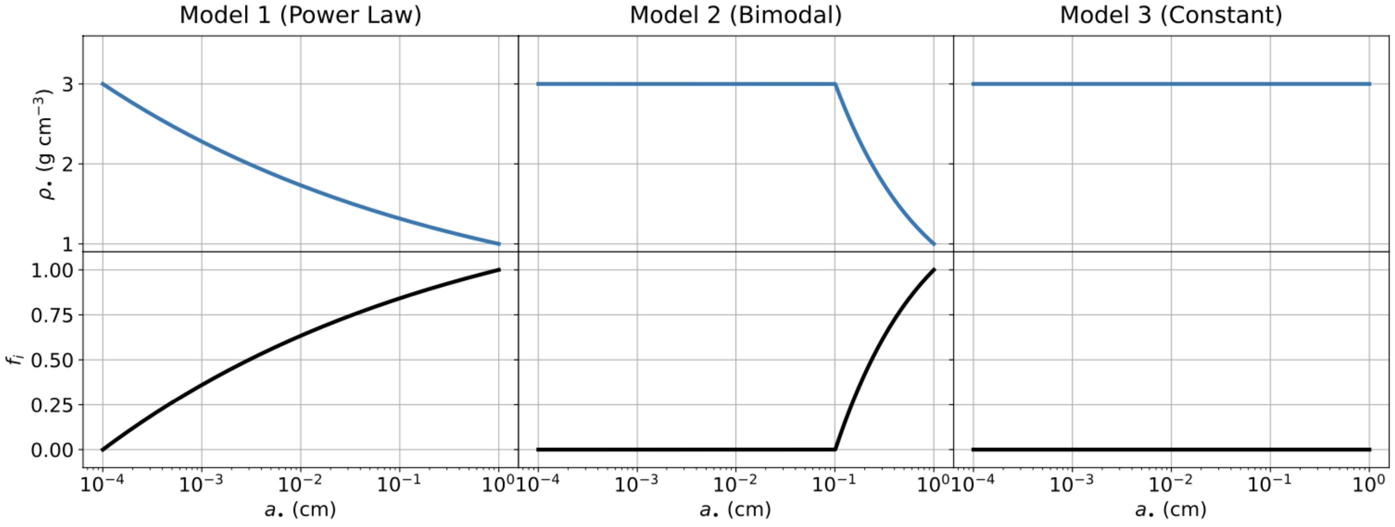

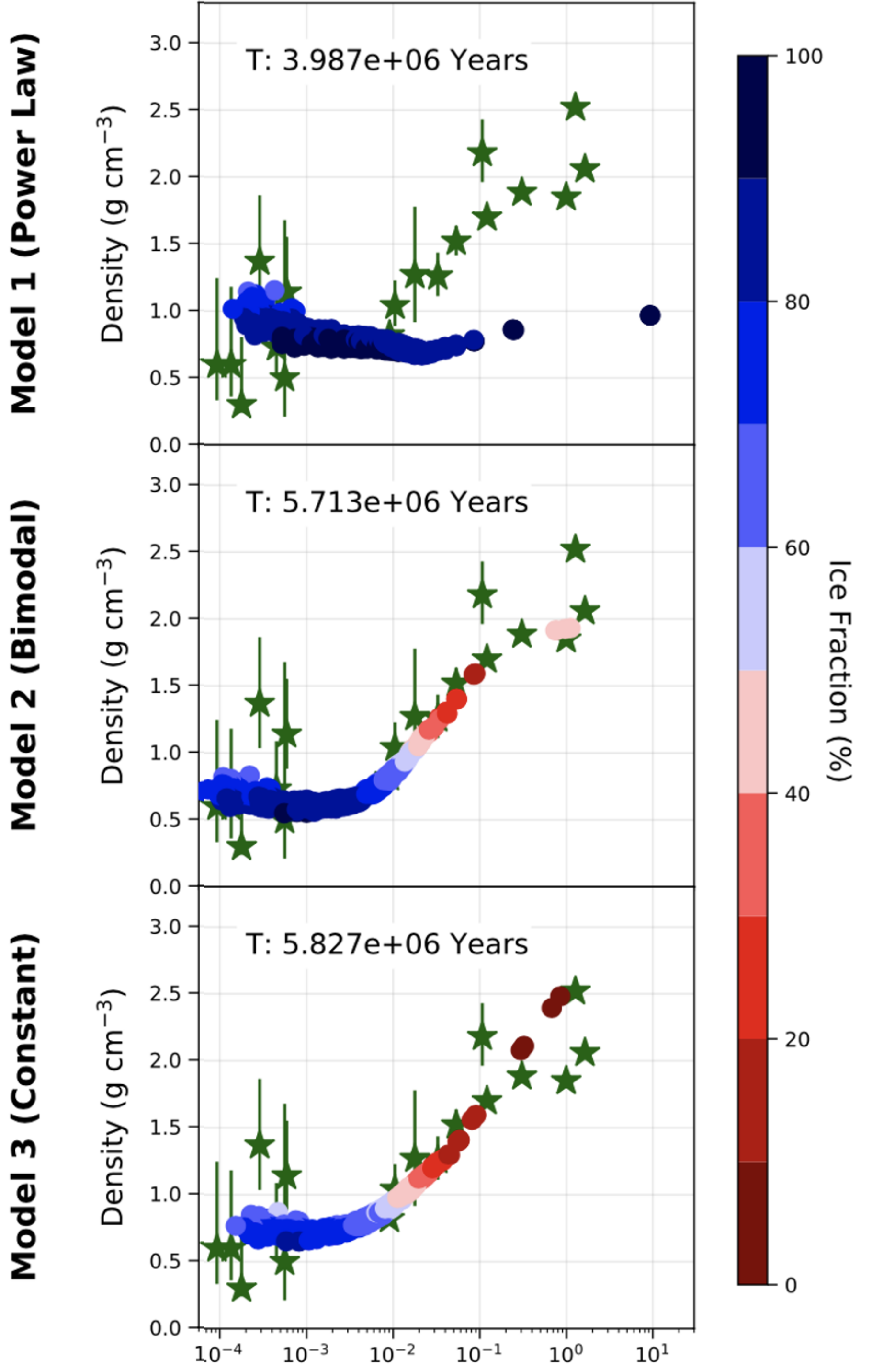

Canas+Lyra et al. 2024

Growing Pluto by silicate pebble accretion

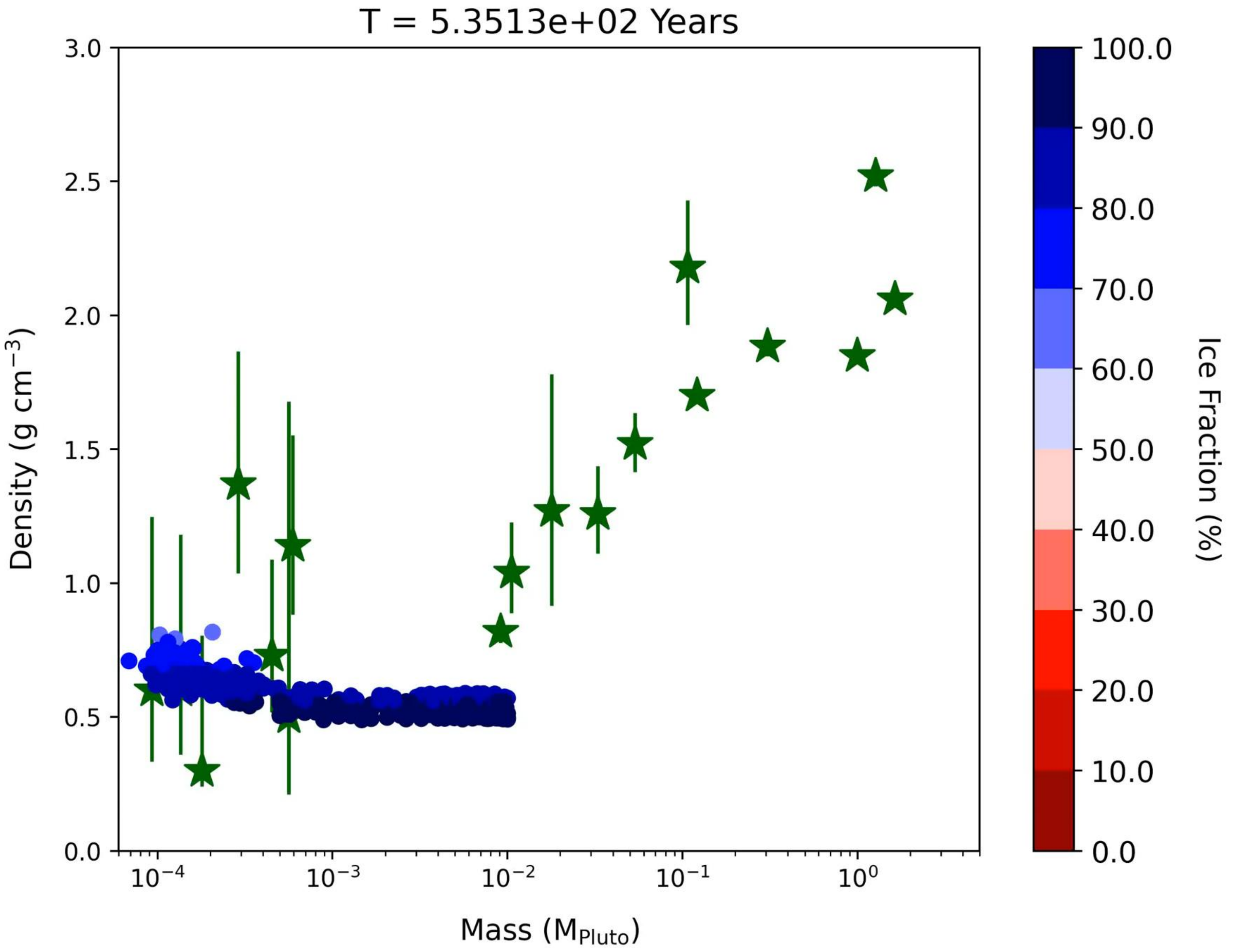

Canas+Lyra et al. 2024

Distance Range
15 - 25AU

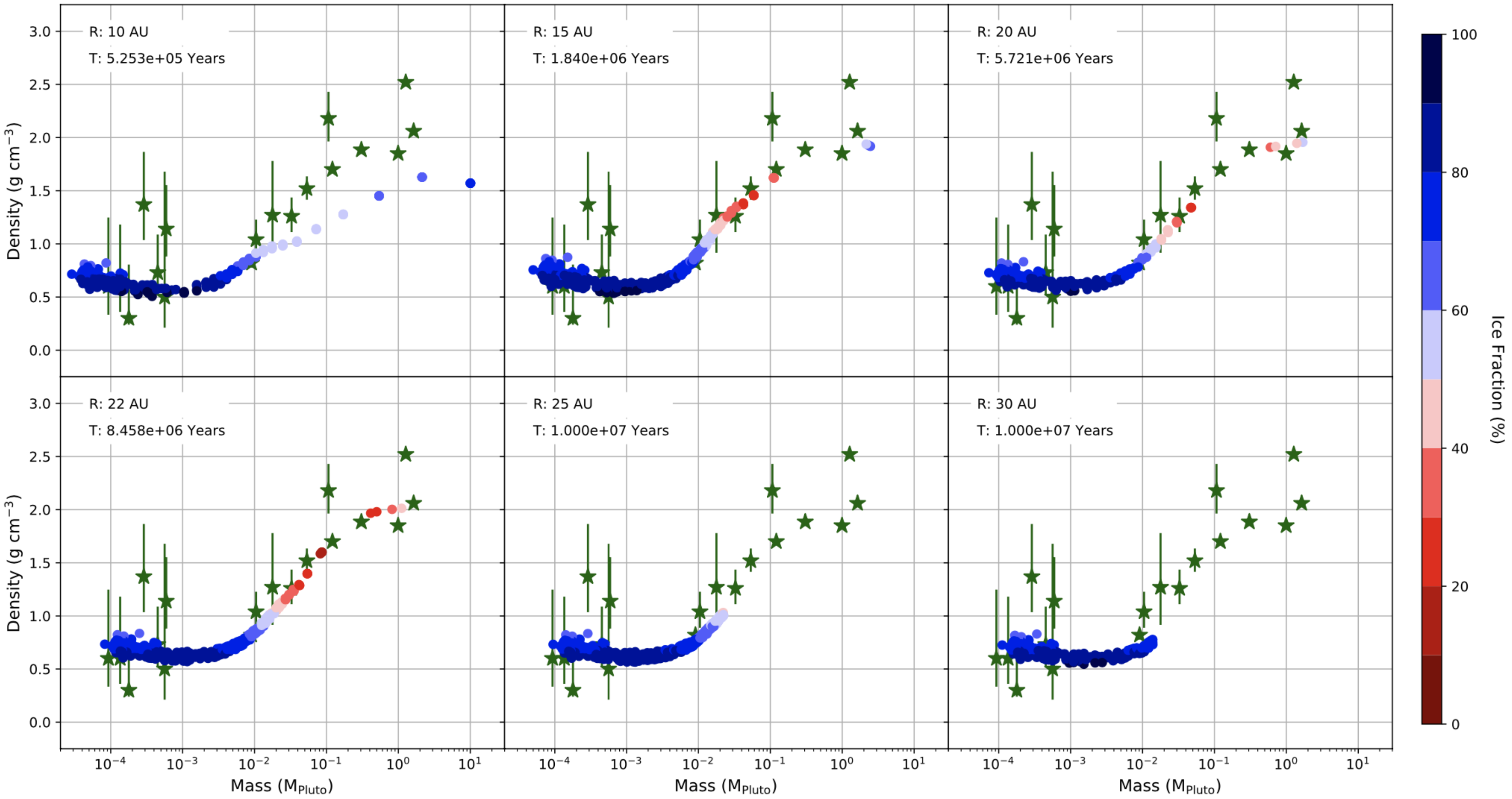

Canas+Lyra et al. 2024

The window of silicate accretion

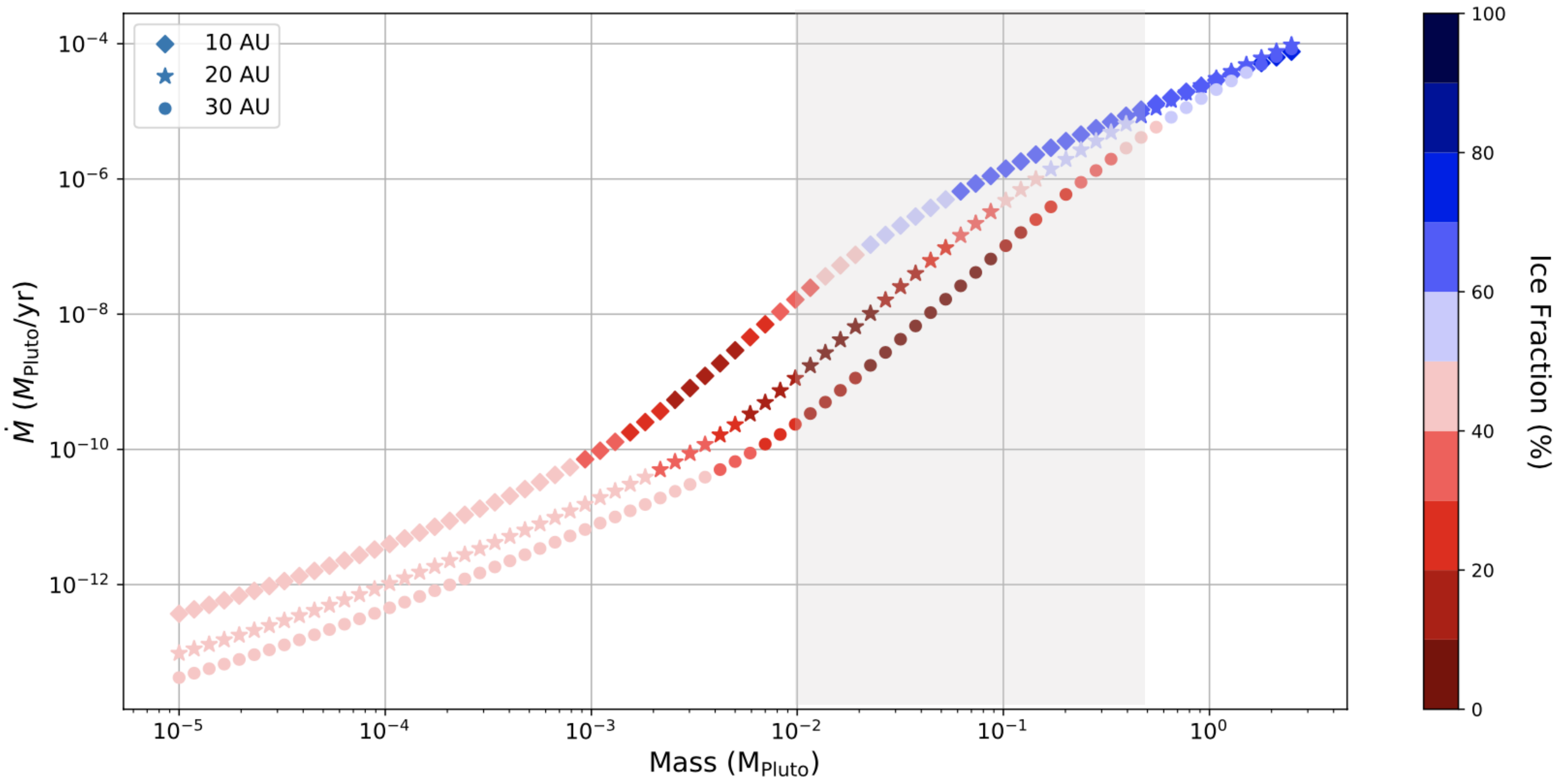

Canas+Lyra et al. 2024

A mass gap

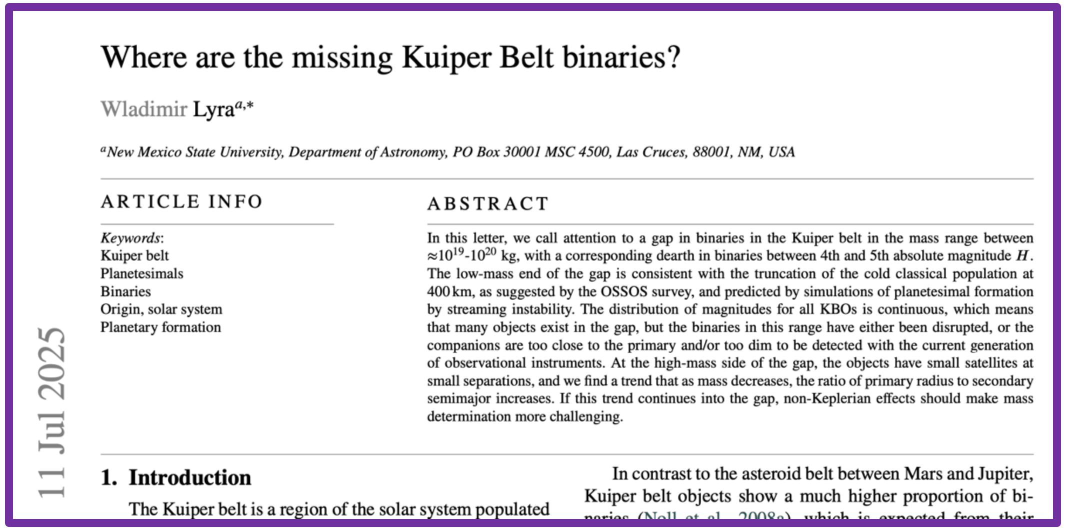

11 Jul 2025

Where are the missing Kuiper Belt binaries?

Wladimir Lyra[a,*]

[a]New Mexico State University, Department of Astronomy, PO Box 30001 MSC 4500, Las Cruces, 88001, NM, USA

ARTICLE INFO

Keywords:
Kuiper belt
Planetesimals
Binaries
Origin, solar system
Planetary formation

ABSTRACT

In this letter, we call attention to a gap in binaries in the Kuiper belt in the mass range between $\approx 10^{19}$-10^{20} kg, with a corresponding dearth in binaries between 4th and 5th absolute magnitude H. The low-mass end of the gap is consistent with the truncation of the cold classical population at 400 km, as suggested by the OSSOS survey, and predicted by simulations of planetesimal formation by streaming instability. The distribution of magnitudes for all KBOs is continuous, which means that many objects exist in the gap, but the binaries in this range have either been disrupted, or the companions are too close to the primary and/or too dim to be detected with the current generation of observational instruments. At the high-mass side of the gap, the objects have small satellites at small separations, and we find a trend that as mass decreases, the ratio of primary radius to secondary semimajor increases. If this trend continues into the gap, non-Keplerian effects should make mass determination more challenging.

1. Introduction

The Kuiper belt is a region of the solar system populated

In contrast to the asteroid belt between Mars and Jupiter, Kuiper belt objects show a much higher proportion of bi-

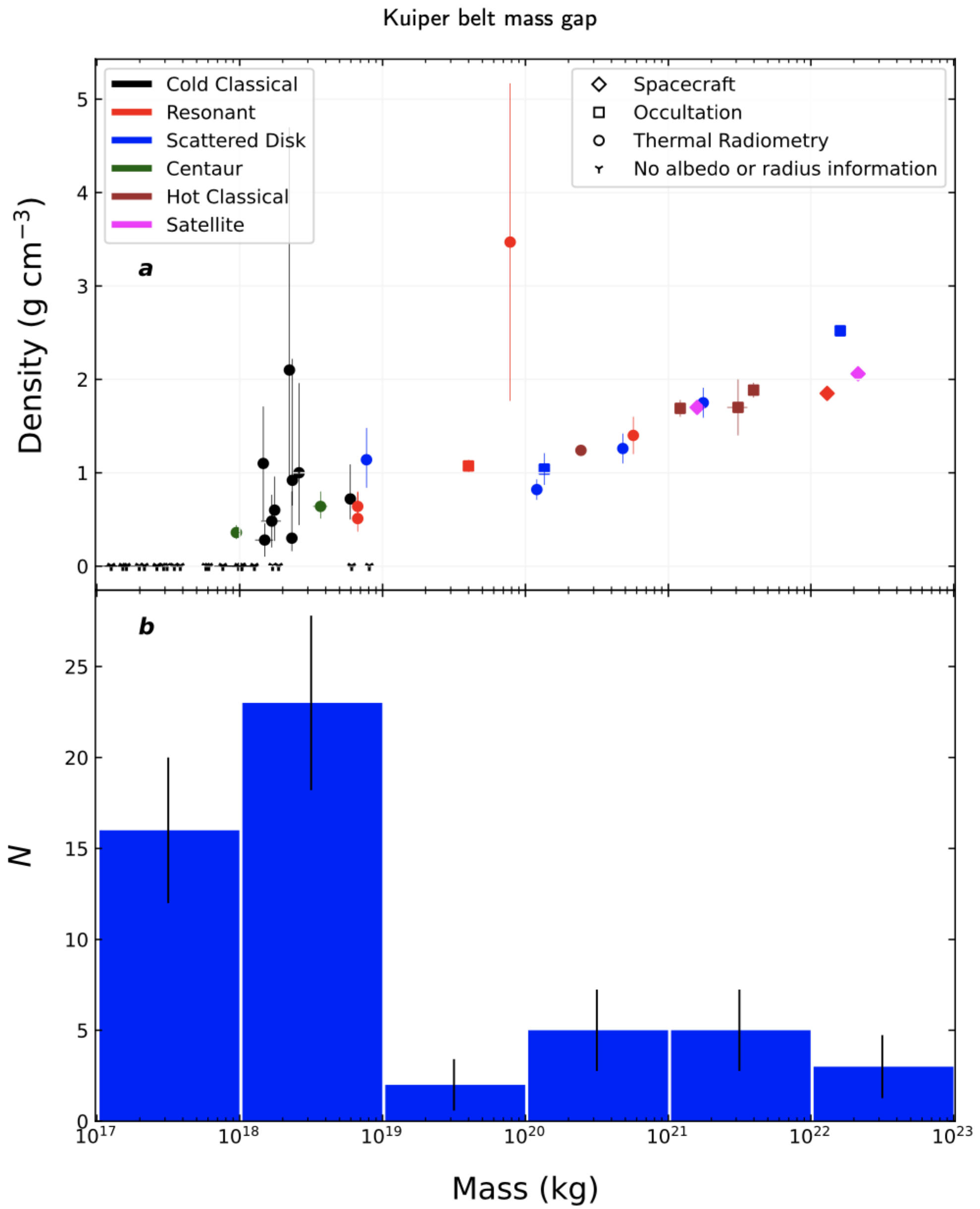

Lyra (2025)

Low-mass end: consistent with high-mass end of Streaming Instability

A&A 597, A69 (2017)
DOI: 10.1051/0004-6361/201629561

Astronomy & Astrophysics

Initial mass function of planetesimals formed by the streaming instability

Urs Schäfer[1,2], Chao-Chin Yang[2], and Anders Johansen[2]

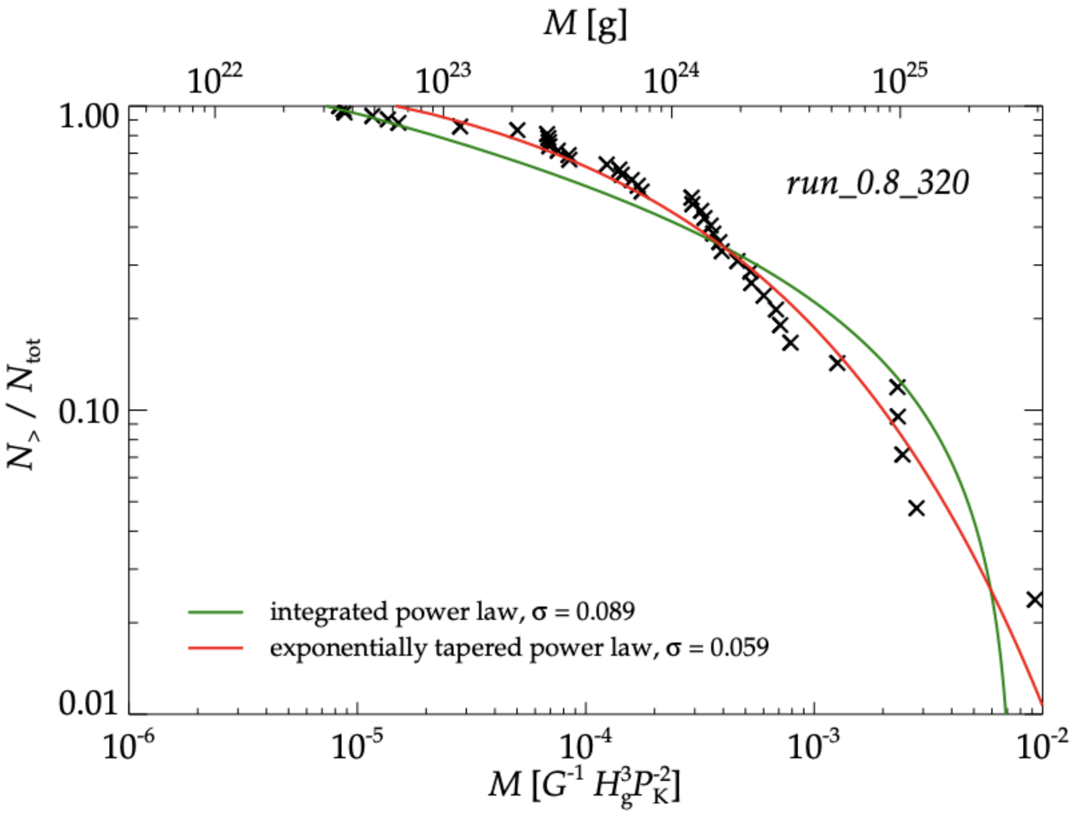

Schafer et al. (2017)

The Astrophysical Journal Letters, 920:L28 (7pp), 2021 October 20
https://doi.org/10.3847/2041-8213/ac2c72

CrossMark

OSSOS Finds an Exponential Cutoff in the Size Distribution of the Cold Classical Kuiper Belt

J. J. Kavelaars[1,2,3], Jean-Marc Petit[4], Brett Gladman[3], Michele T. Bannister[5], Mike Alexandersen[6], Ying-Tung Chen[7], Stephen D. J. Gwyn[1], and Kathryn Volk[8]

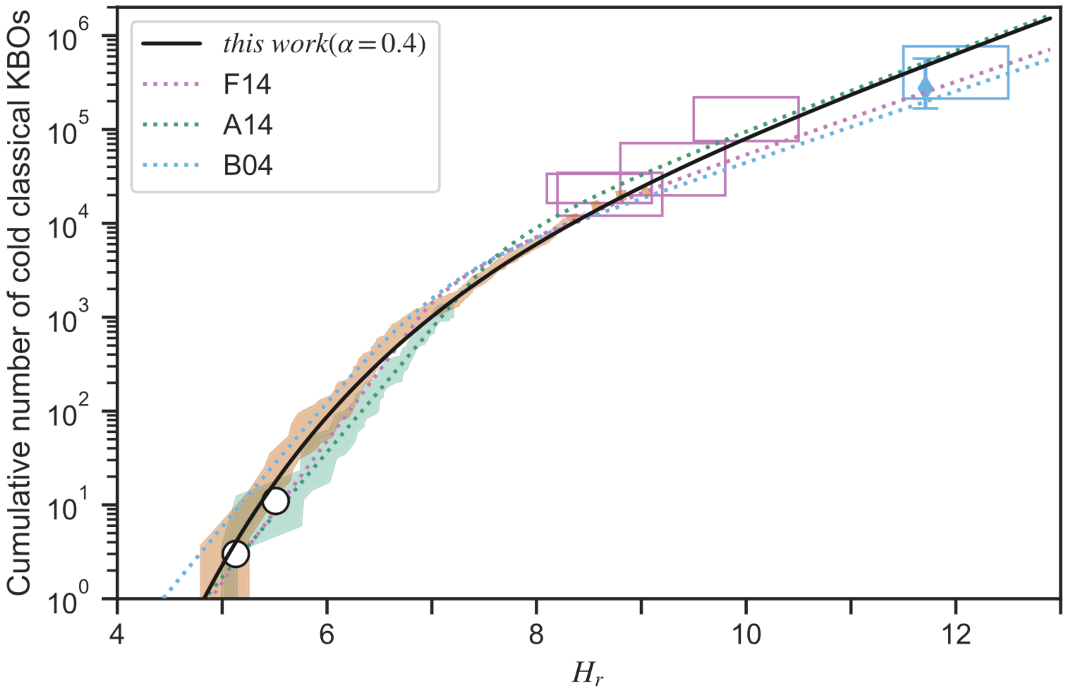

Figure 2. As in Figure 1, the orange region represents the debiased OSSOS++ sample. The green shaded area represents the debiased detections from the Deep Ecliptic Survey (Adams et al. 2014), with the green dotted line indicating the best-fit double exponential. Also shown are the best fits from Bernstein et al. (2004; cyan dotted line) and Fraser et al. (2014; magenta dotted line). The curves have been scaled to reflect the difference in survey filters and for differences in selection function for cold classical KBOs. In particular, we use $(r - R) = 0.25$ (Jordi et al. 2006) for $(V - R) = 0.6$ cold classical KBOs, and we scale the apparent magnitude distribution given in B04 using a fixed distance of 42 au to transform from r to H_r. The A14 total population is slightly low compared to the OSSOS++ sample; this may be due to tracking losses reported in A14. The F14 fit has been scaled to match the OSSOS++ sample at $H_r = 8$, as we were uncertain of the scaling from the surface density reported in F14 and the absolute total numbers reported here.

Kavelaars et al (2021)

High-mass side. Observational bias?

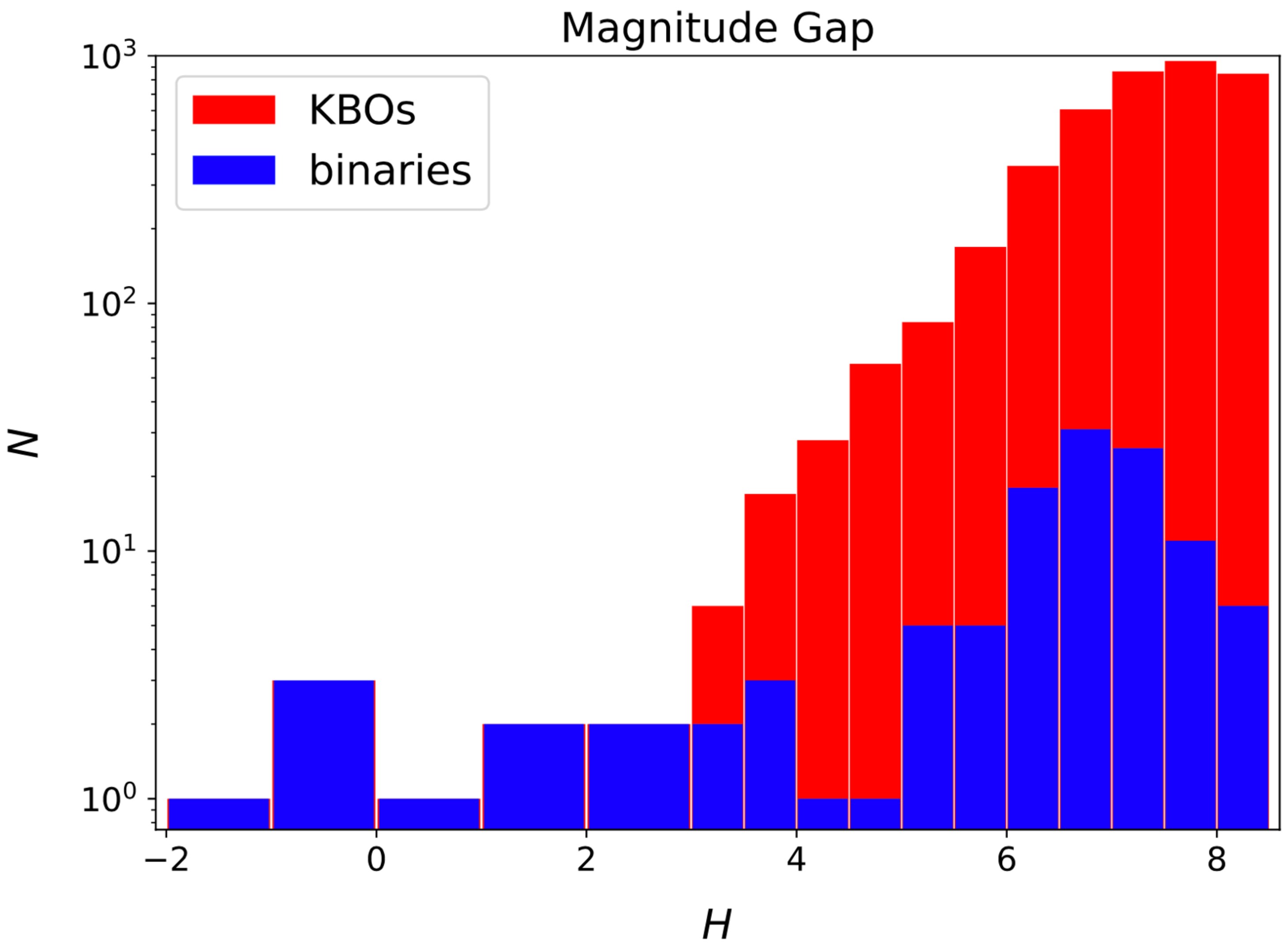

Lyra (2025)

Different system architecture

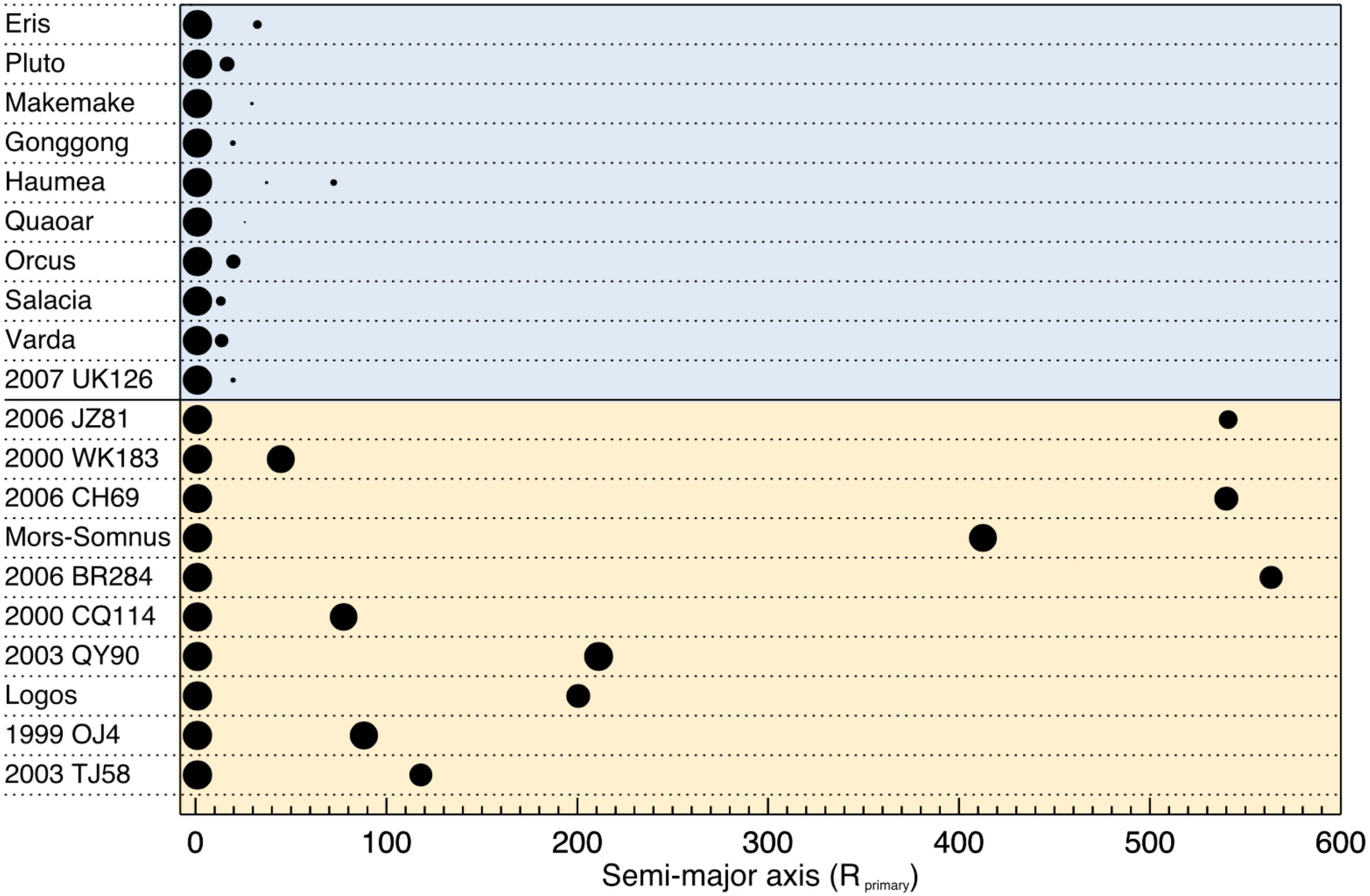

Small satellites, tight orbits

Equal mass, wide binaries

Bernstein et al (2023)

Did the high-mass objects lose their primordial satellites?

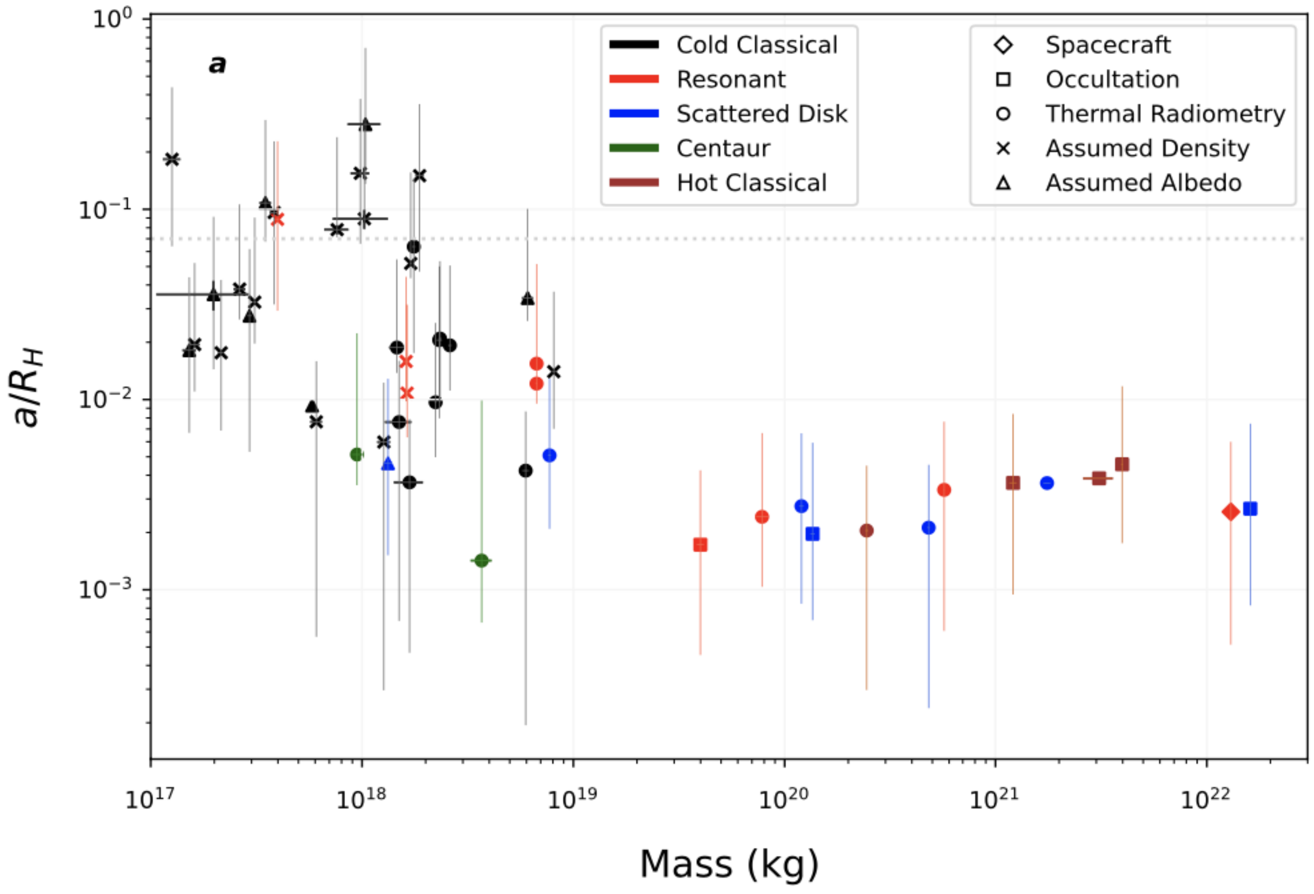

UWBs

Lyra (2025)

Non-Keplerian orbits

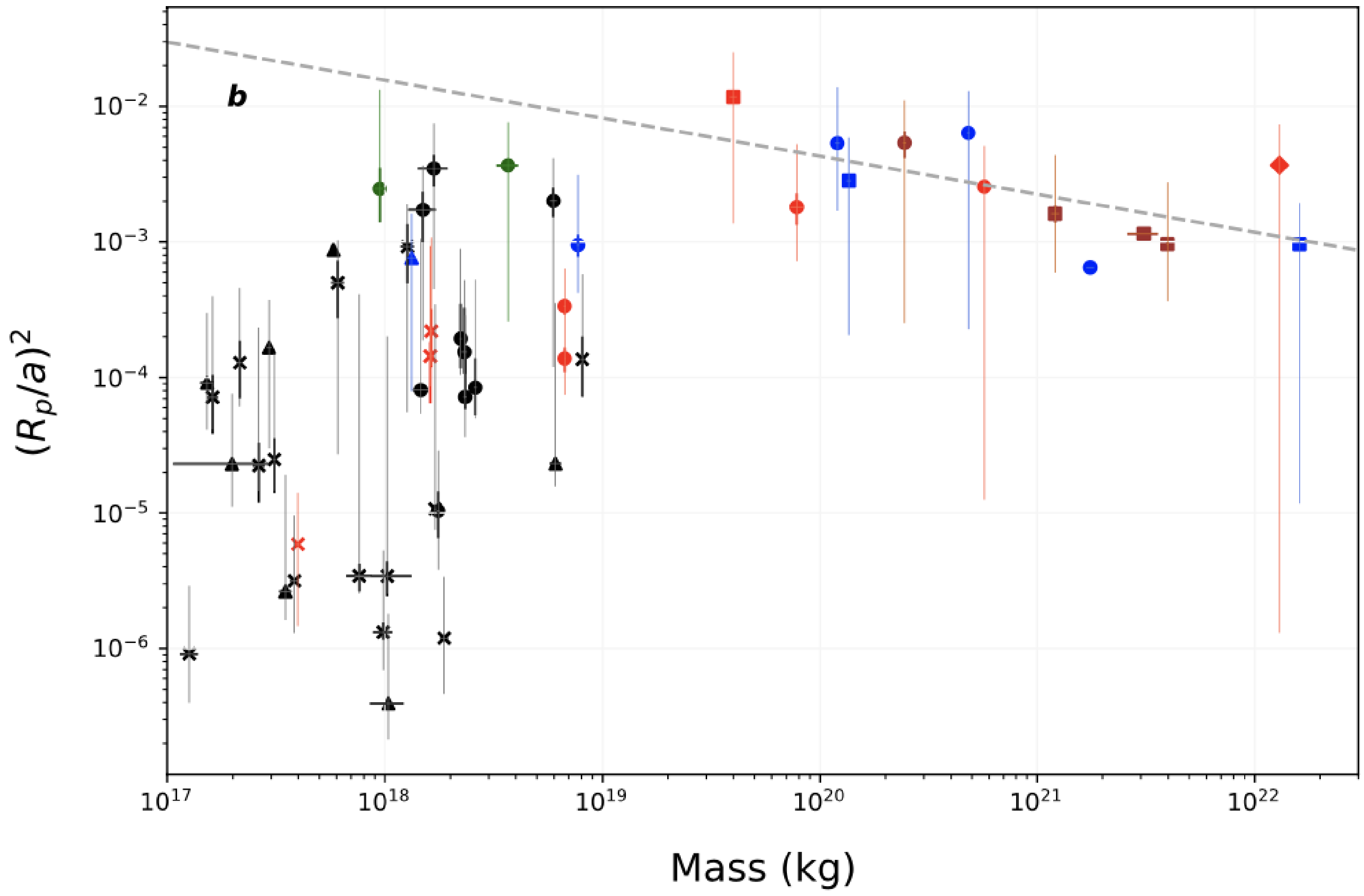

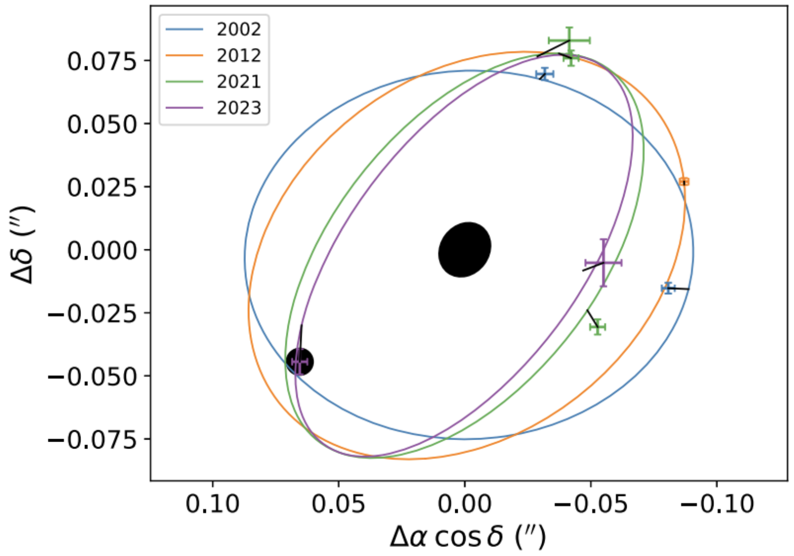

Rommel et al. (2025)

Lyra (2025)

Satellites

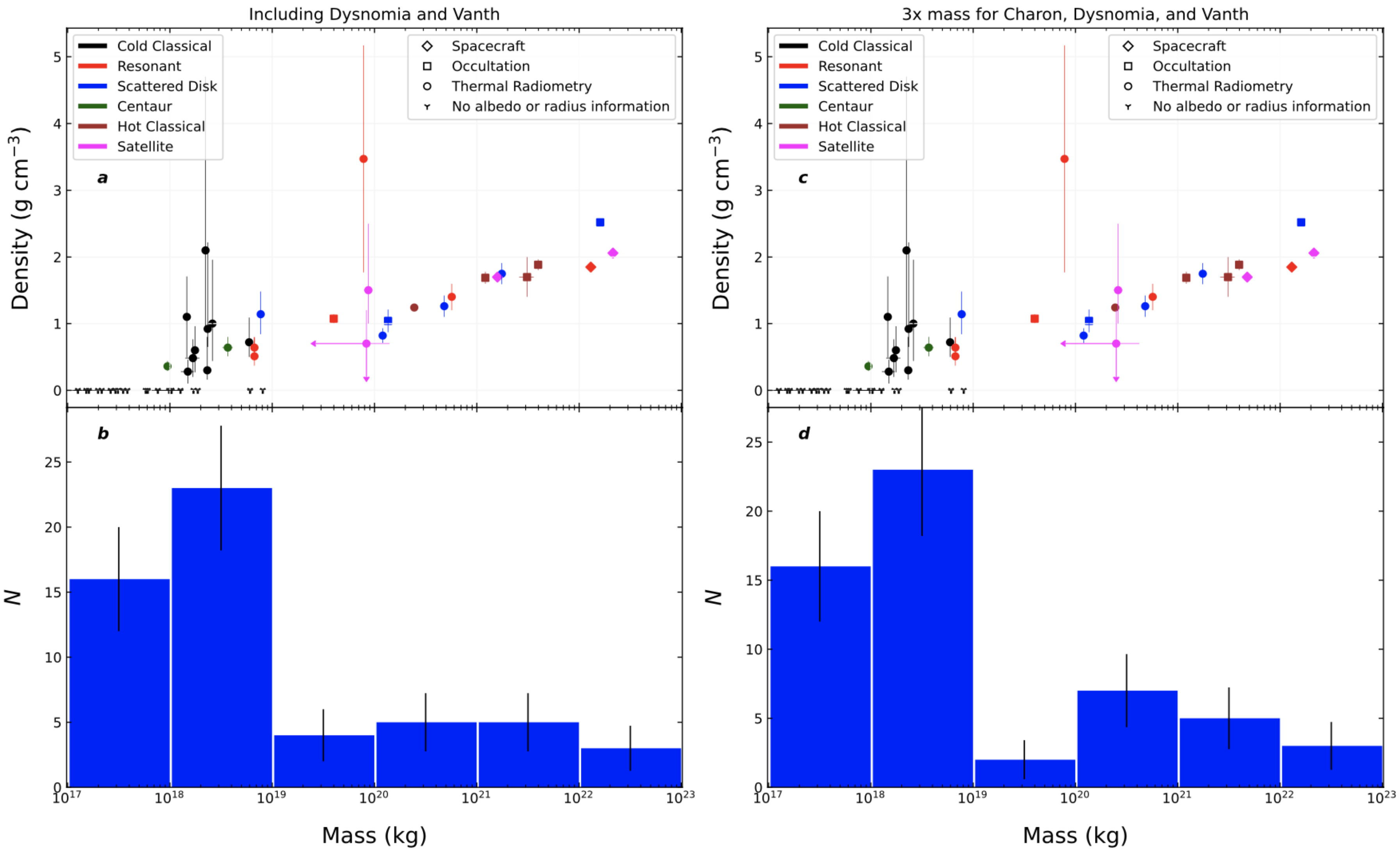

Lyra (2025, but see Denton et al. 2025 for lower mass ratios)

Arrokoth

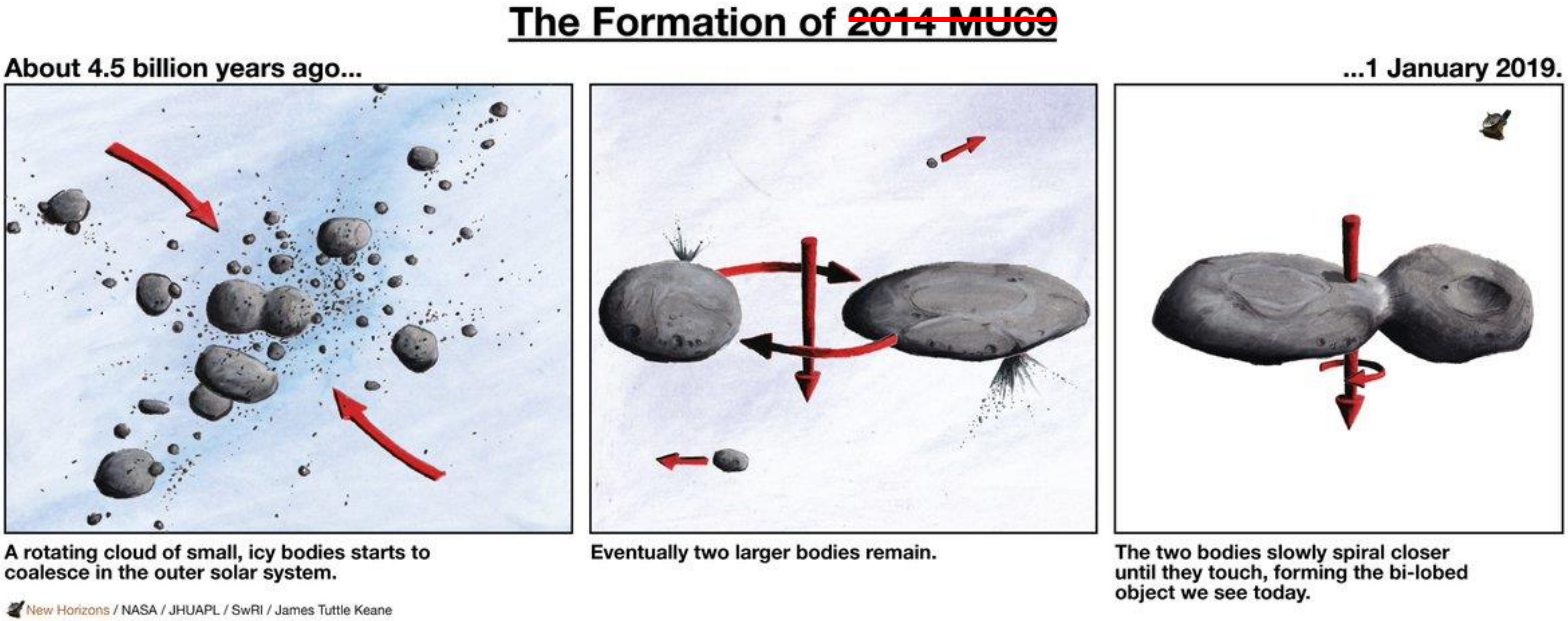

Sketch by J.T. Keane

Wind

Solar orbit velocity at 45AU

$\boldsymbol{v_k \sim 4.5}$ **km/s**

Sub-Keplerian pressure support

$v = v_k (1-\eta)$

$\eta \sim 0.01$

Headwind velocity (v_k-v):

$\eta v \sim 50$ ***m/s***

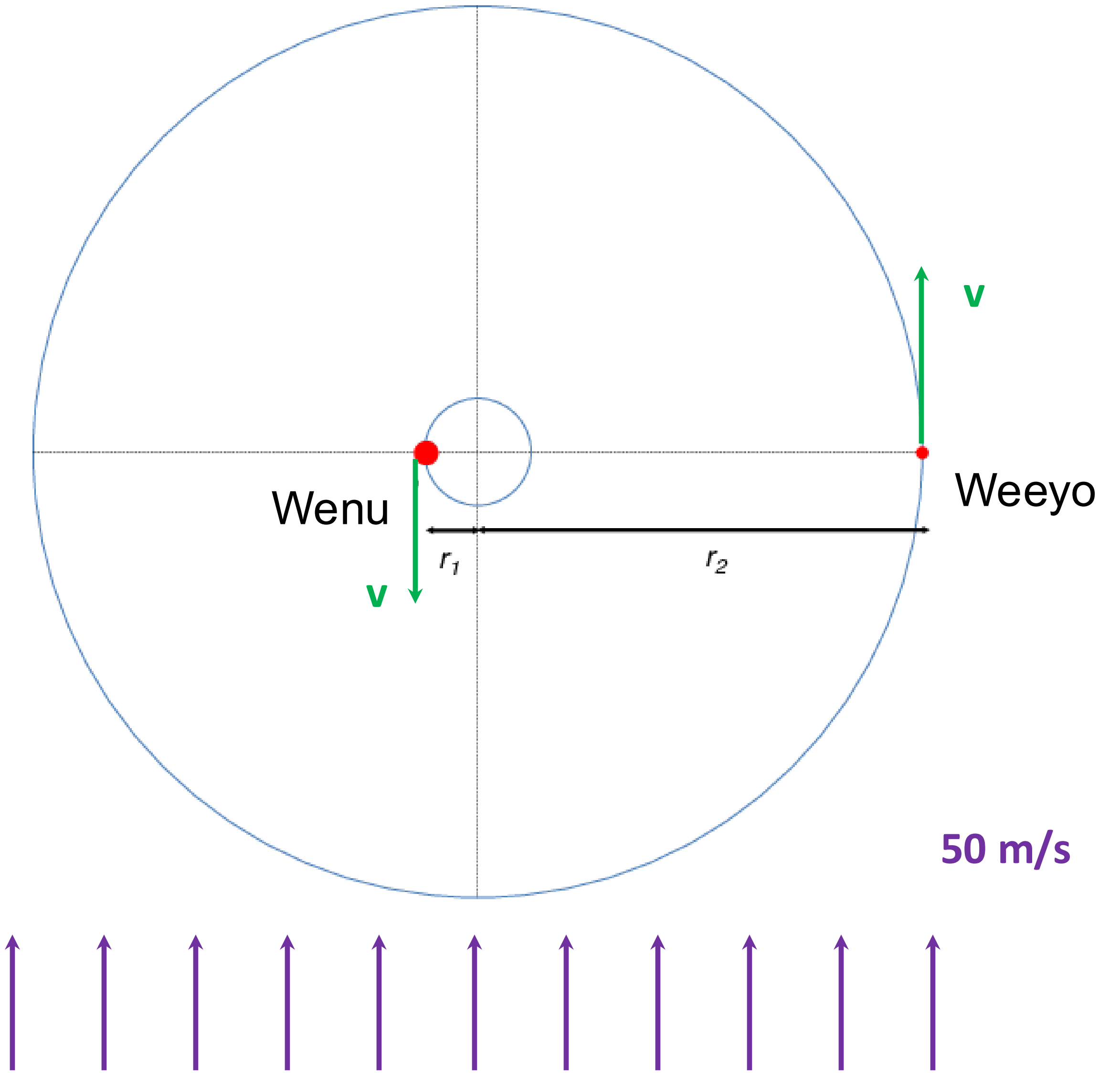

Lyra et al. (2021)

Wind solution

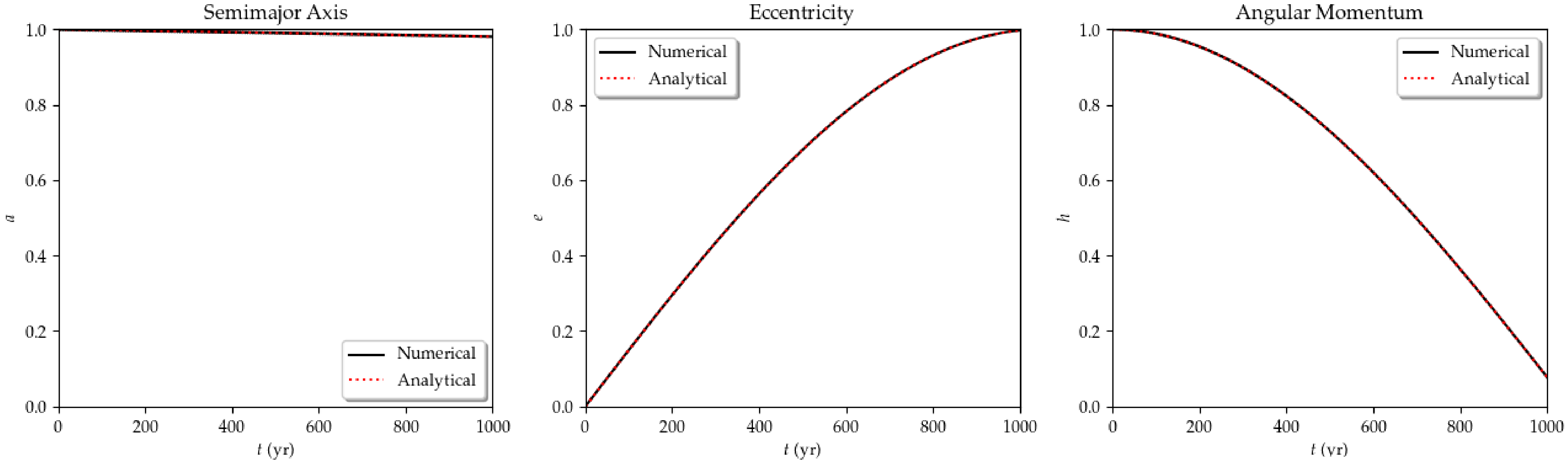

$$\langle a(t)\rangle = a_0 e^{-2t/\tau}$$

$$\langle e(t)\rangle = \cos\left[\cos^{-1} e_0 + \frac{3u}{2}\sqrt{\frac{a_0}{\mu}}\left(1-e^{-t/\tau}\right)\right]$$

$$\langle h(t)\rangle = e^{-t/\tau}\left\{h_0 - 1 + \cos\left[\frac{3}{2}a_0 u\left(1-e^{-t/\tau}\right)\right]\right\}$$

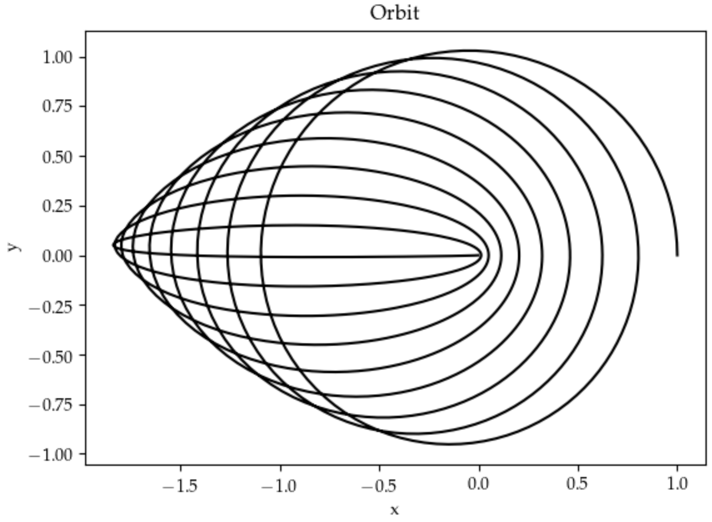

W. Lyra

Lyra et al. (2021)

Timescales

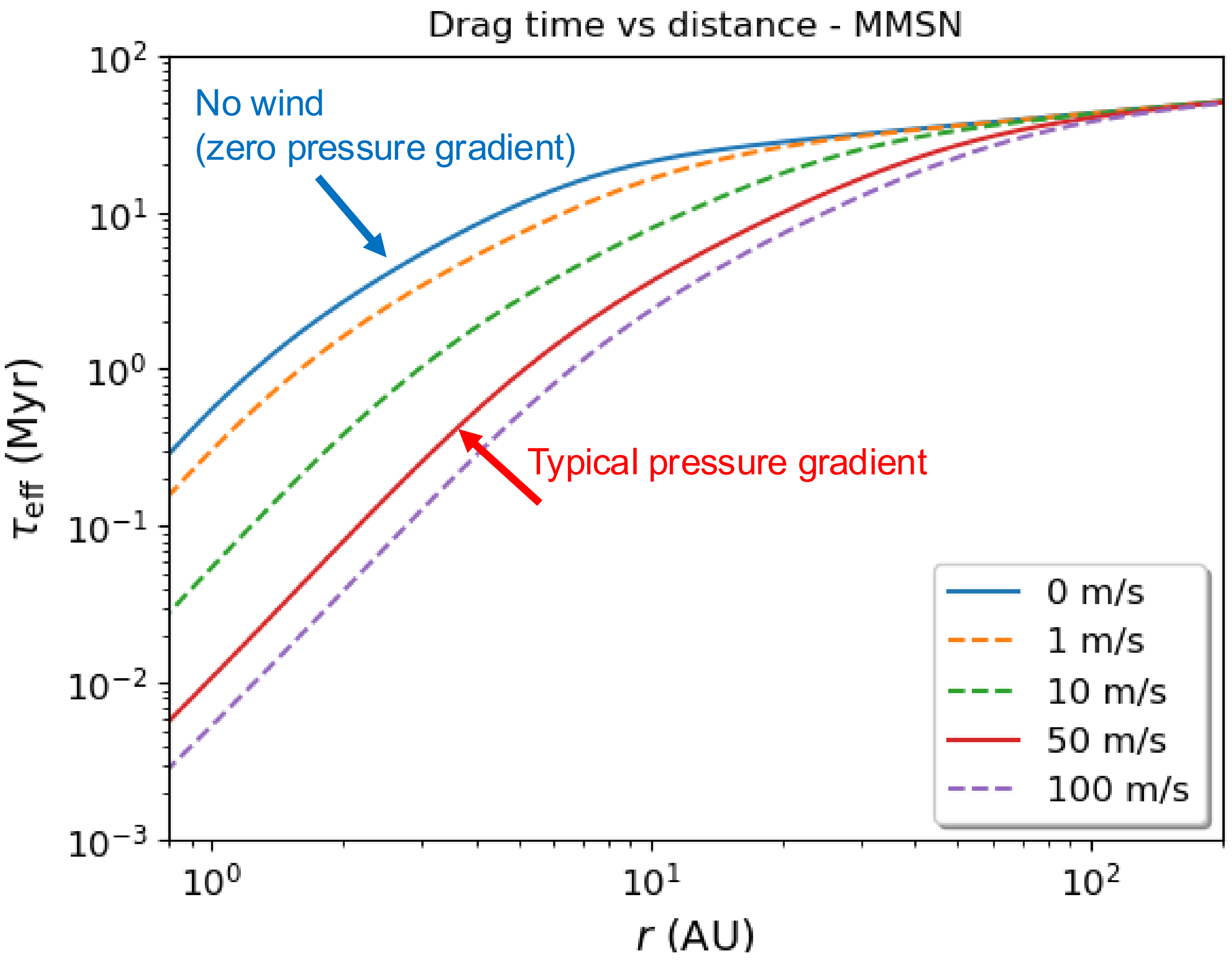

Wind has a strong effect in the inner disk.

Little effect for Arrokoth

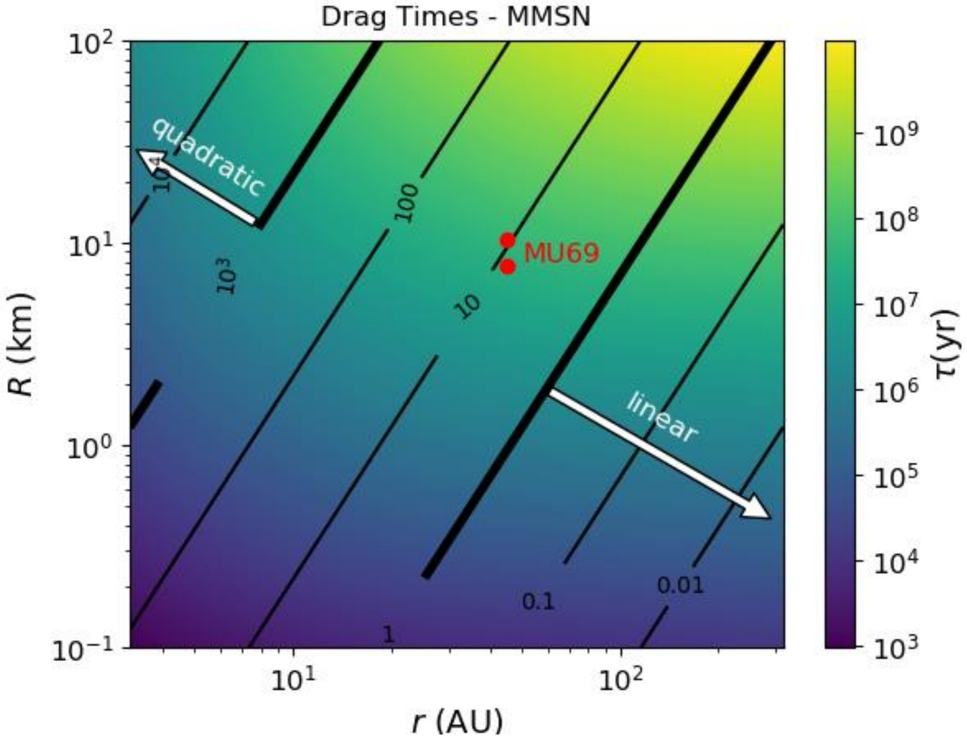

Lyra et al. (2021)

Kozai-Lidov Oscillations

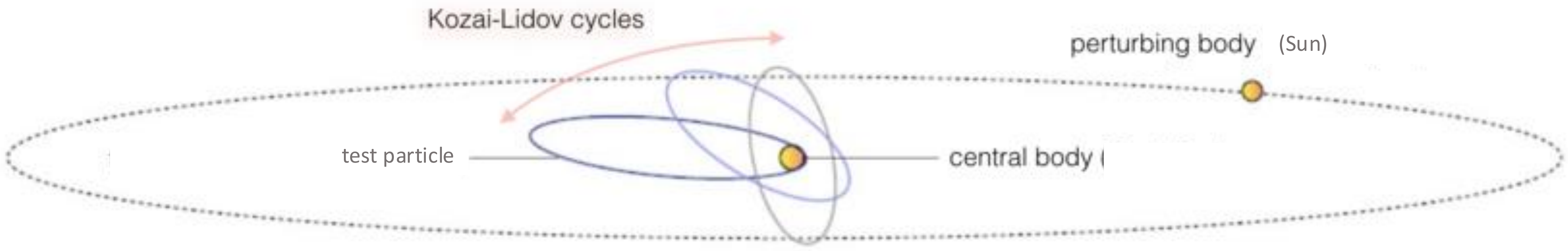

Lyra et al. (2021)

Kozai + Tidal Friction + Drag

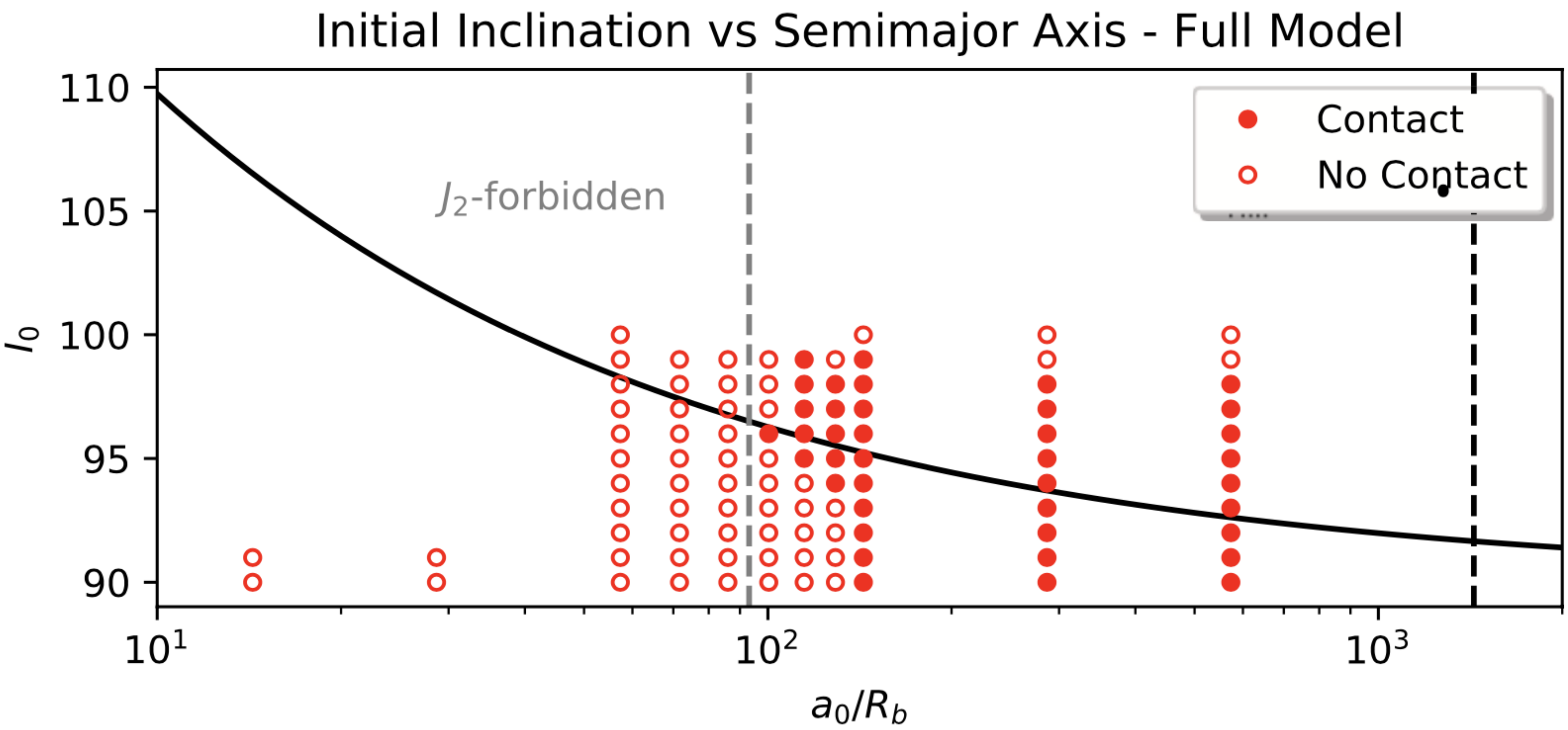

Lyra et al. (2021)

Effect of Drag on Kozai cycles

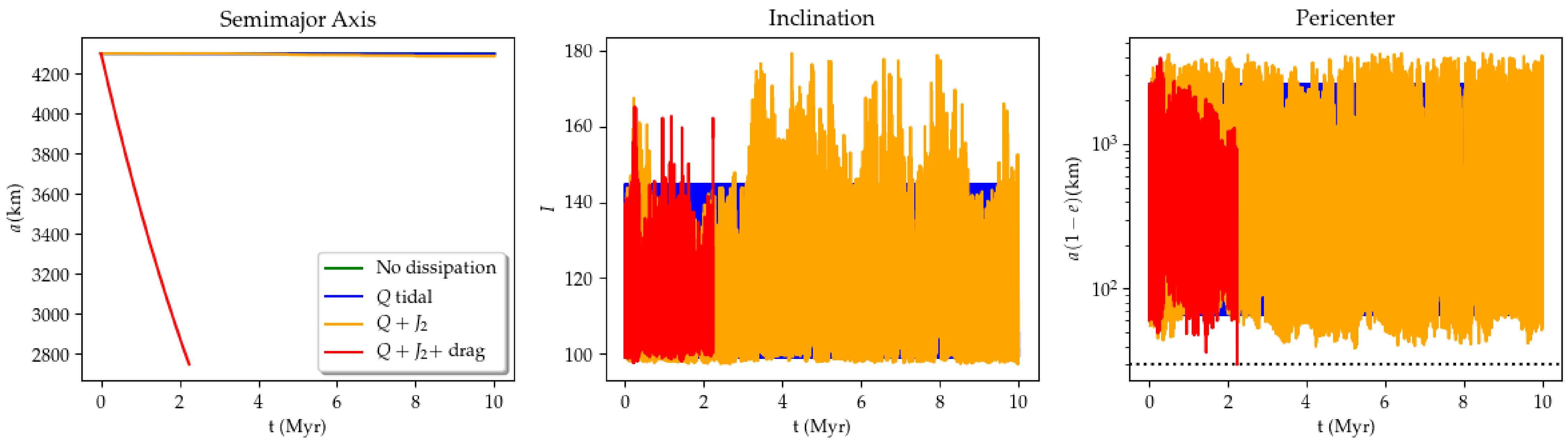

Lyra et al. (2021)

Conclusions

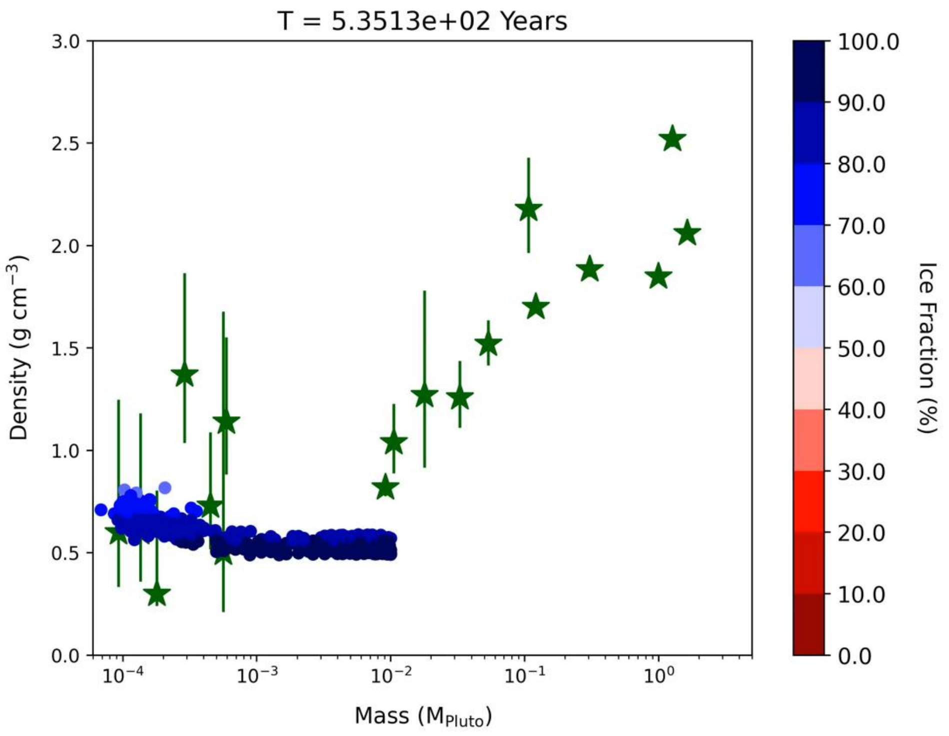

- KBO density problem:
  - Two different pebble populations, maintained by ice desorption off small grains
  - Streaming instability: icy-rich small objects; nearly uniform composition
  - Pebble accretion: silicate-rich larger objects; varied composition
  - Melting avoided by
    - ice-rich formation
    - ^{26}Al incorporated mostly in long (>Myr) phase of silicate accretion
  - KBOs best reproduced between 15-25 AU

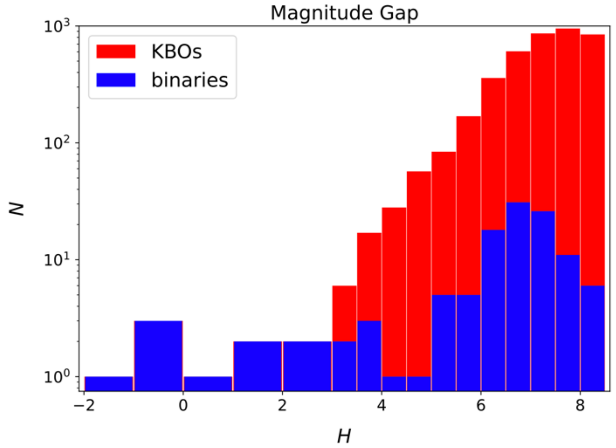

- A gap in KBO binaries
  - Cold classicals capped at 10^{-3} Pluto masses
  - Gap between 10^{-3} and 10^{-2} Pluto masses for non-cold classicals (4 ~< *H* ~< 5)
    - Formation imprint?
    - Dynamical loss?
    - Observation bias?
    - All of the above?

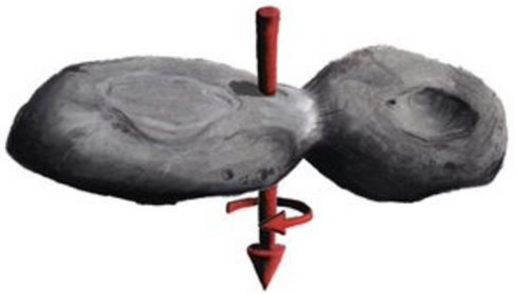

- Arrokoth
  - Solved the binary planetesimal problem with gas drag
  - Implemented the solution into a Kozai plus tidal friction code
  - Window of contact increased by combined effect of J_2 and drag
  - Contact via Kozai cycles in the Kuiper belt, orbits become grazing
  - ~ 10% of KBCC binaries should be contact binaries

EXTRA SLIDES

The first planetesimals won't melt

$$\mathcal{H} = \rho\, F_s\, [^{26}\mathrm{Al}]_0\, \mathcal{H}_0\, e^{-\lambda t}$$

$$Q(t) = V \int_0^t \mathcal{H}(t')dt'$$

$$= M_p\, F_s\, [^{26}\mathrm{Al}]_0\, \mathcal{H}_0\, \lambda^{-1} \left(1 - e^{-\lambda t}\right)$$

$$Q = M_p\, c_p\, \Delta T$$

$$\Delta T = F_s\, [^{26}\mathrm{Al}]_0\, \mathcal{H}_0\, \lambda^{-1}\, c_p^{-1}$$

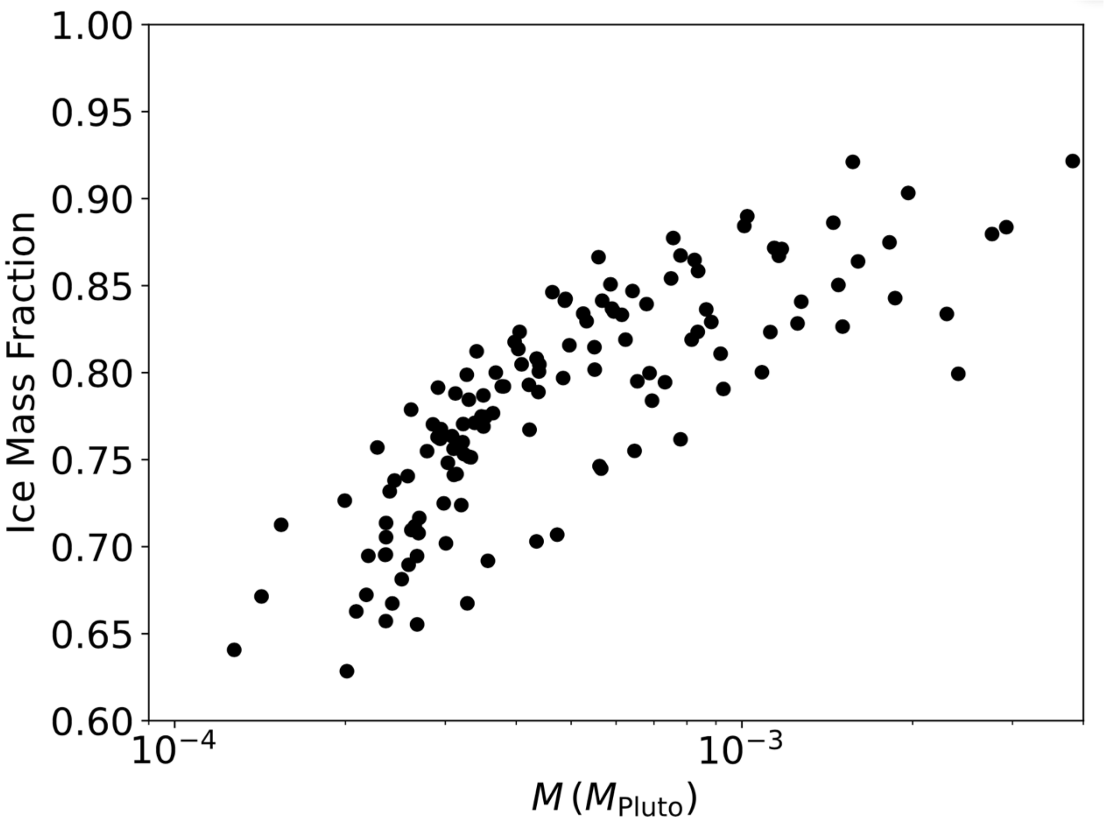

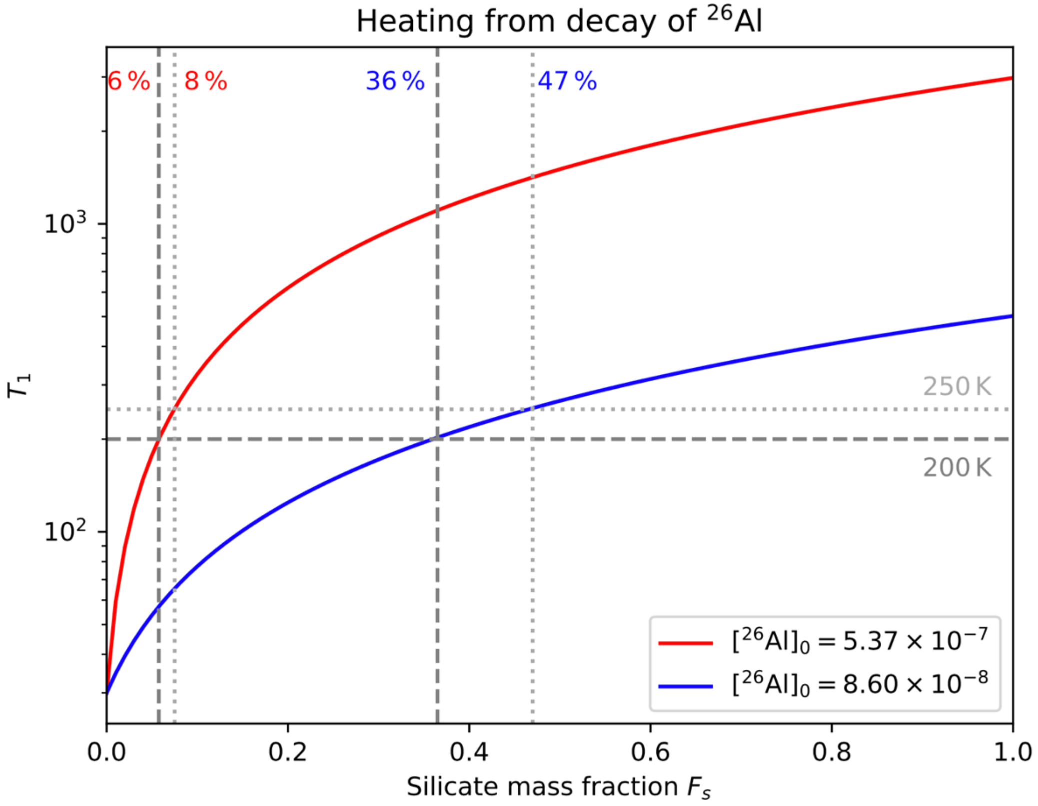

Canas+Lyra et al. 2024

Polydisperse (Multi-Species) Pebble Accretion

$$\rho_d(a,z) = \int_0^a m(a')\,F(a',z)\,da'.$$

$$F(a,z) \equiv f(a)\,e^{-z^2/2H_d^2},$$

$$f(a) = \frac{3(1-p)Z\Sigma_g}{2^{5/2}\pi^{3/2}H_g\rho_\bullet^{(0)}a_{\rm max}^{4-k}}\sqrt{1+a\frac{\pi}{2}\frac{\rho_\bullet(a)}{\Sigma_g\alpha}}\;a^{-k}.$$

$$\dot{M}(a) = \int_0^a \frac{\partial\dot{M}(a')}{\partial a'}da',$$

$$\frac{\partial\dot{M}(a)}{\partial a} = \pi R_{\rm acc}^2(a)\,\delta v(a)\,S(a)\,m(a)\,f(a).$$

$$S \equiv \frac{1}{\pi R_{\rm acc}^2}\int_{-R_{\rm acc}}^{R_{\rm acc}} 2\sqrt{R_{\rm acc}^2 - z^2}\,\exp\left(-\frac{z^2}{2H_d^2}\right)dz,$$

$$W(a) = \frac{3(1-p)Z\Sigma_g}{4\pi\rho_\bullet^{(0)}a_{\rm max}^{4-k}}\,a^{-k},$$

$$\delta v \equiv \Delta v + \Omega R_{\rm acc},$$

$$R_{\rm acc} \equiv \hat{R}_{\rm acc}\exp[-\chi(\tau_f/t_p)^\gamma],$$

$$\hat{R}_{\rm acc}^{\rm (Bondi)} = \left(\frac{4\tau_f}{t_{\rm B}}\right)^{1/2}R_{\rm B},$$

$$\hat{R}_{\rm acc}^{\rm (Hill)} = \left(\frac{\rm St}{0.1}\right)^{1/3}R_{\rm H},$$

$$\frac{\partial\Sigma_d(a)}{\partial a} \propto a^{-p};$$

$$\rho_\bullet \propto a^{-q};$$

$$t_p \equiv \frac{GM_p}{(\Delta v + \Omega R_{\rm H})^3}$$

$$\dot{M}_{\rm 2D,\,Hill} = 2\times 10^{2/3}\Omega R_H^2\int_0^{a_{\rm max}} {\rm St}(a)^{2/3}\,m(a)\,W(a)\,da.$$

$$\dot{M}_{\rm 3D,\,Bondi} = \frac{4\pi R_{\rm B}\Delta v^2}{\Omega}\times\int_0^{a_{\rm max}}{\rm St}\,e^{-2\psi}m(a)f(a)\times\left[1+2\left({\rm St}\frac{\Omega R_{\rm B}}{\Delta v}\right)^{1/2}e^{-\psi}\right]da,$$

$$\psi \equiv \chi[{\rm St}/(\Omega t_p)]^\gamma.$$

Lyra et al. 2023

Analytical theory of polydisperse (multi-species) pebble accretion

$\xi \equiv \left(\frac{R_{acc}}{2H_d}\right)^2$

Monodisperse (single species)

$$\dot{M}_{3D} = \lim_{\xi \to 0} \dot{M} = \pi R_{acc}^2 \rho_{d0} \delta v,$$

$$\dot{M}_{2D} = \lim_{\xi \to \infty} \dot{M} = 2 R_{acc} \Sigma_d \delta v,$$

Lambrechts & Johansen (2012)

Polydisperse (multiple species)

$$\dot{M}_{2D,Hill} = \frac{6(1-p)}{14-5q-3k}\left(\frac{St_{max}}{0.1}\right)^{2/3} \Omega R_H^2 Z \Sigma_g.$$

$$\dot{M}_{3D,Bondi} \approx C_1 \frac{\gamma_l\left(\frac{b_1+1}{s}, j_1 a_{max}^s\right)}{s j_1^{(b_1+1)/s}} + C_2 \frac{\gamma_l\left(\frac{b_2+1}{s}, j_2 a_{max}^s\right)}{s j_2^{(b_2+1)/s}} + C_3 \frac{\gamma_l\left(\frac{b_3+1}{s}, j_3 a_{max}^s\right)}{s j_3^{(b_3+1)/s}} + C_4 \frac{\gamma_l\left(\frac{b_4+1}{s}, j_4 a_{max}^s\right)}{s j_4^{(b_4+1)/s}},$$

Lyra et al. (2023)

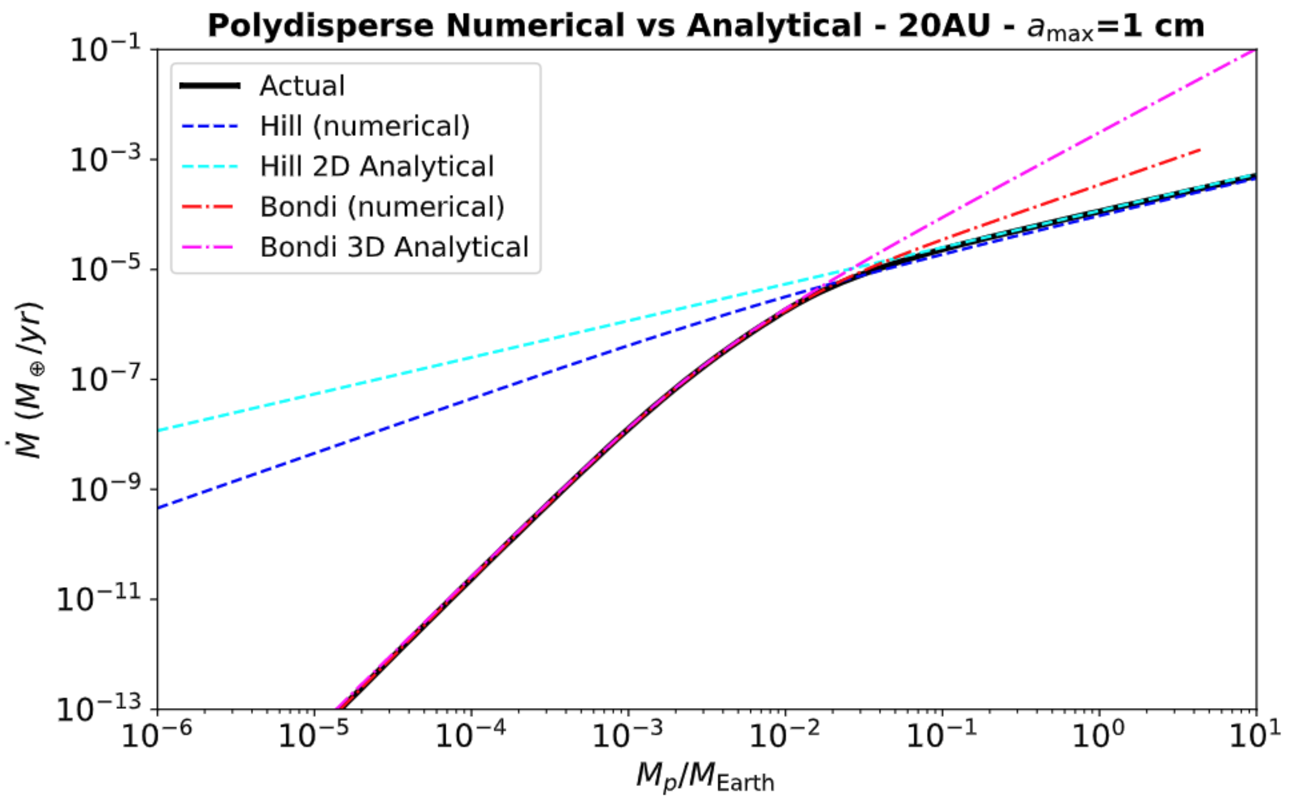

Lyra et al. 2023

Pebble Internal Density

Ice Volume Fraction

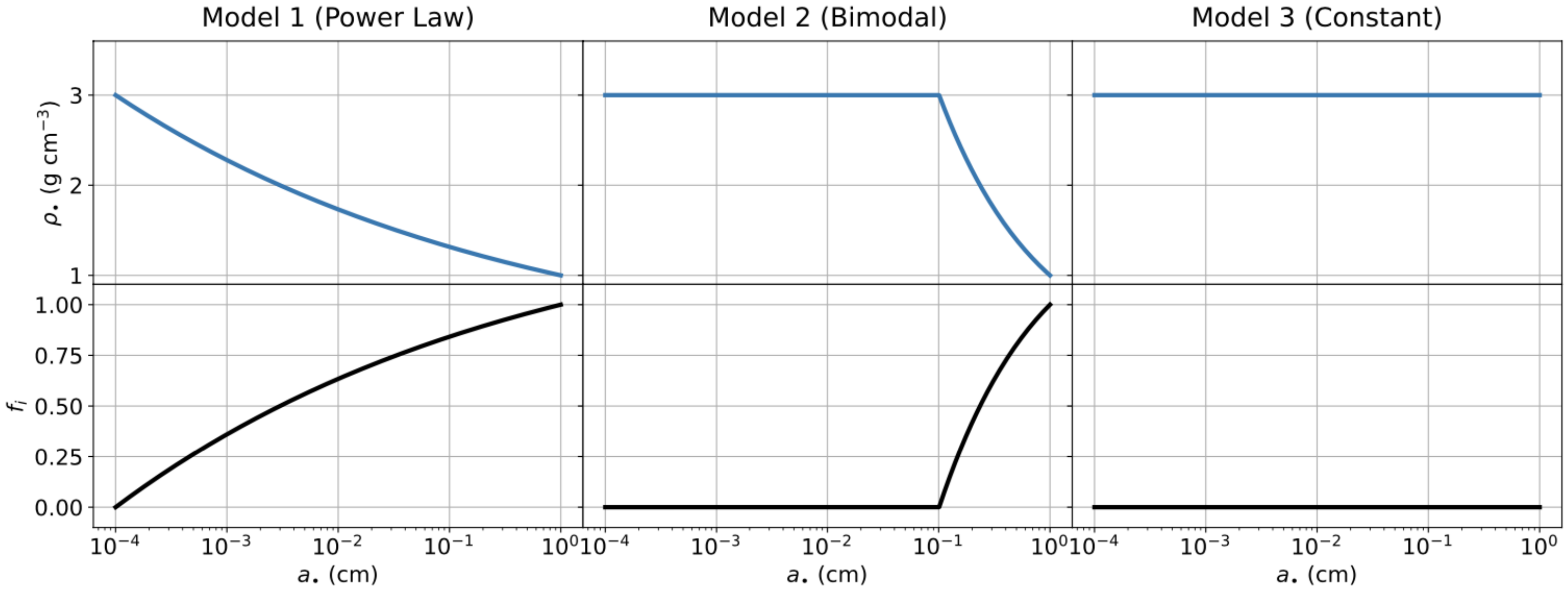

Mass Accretion rate

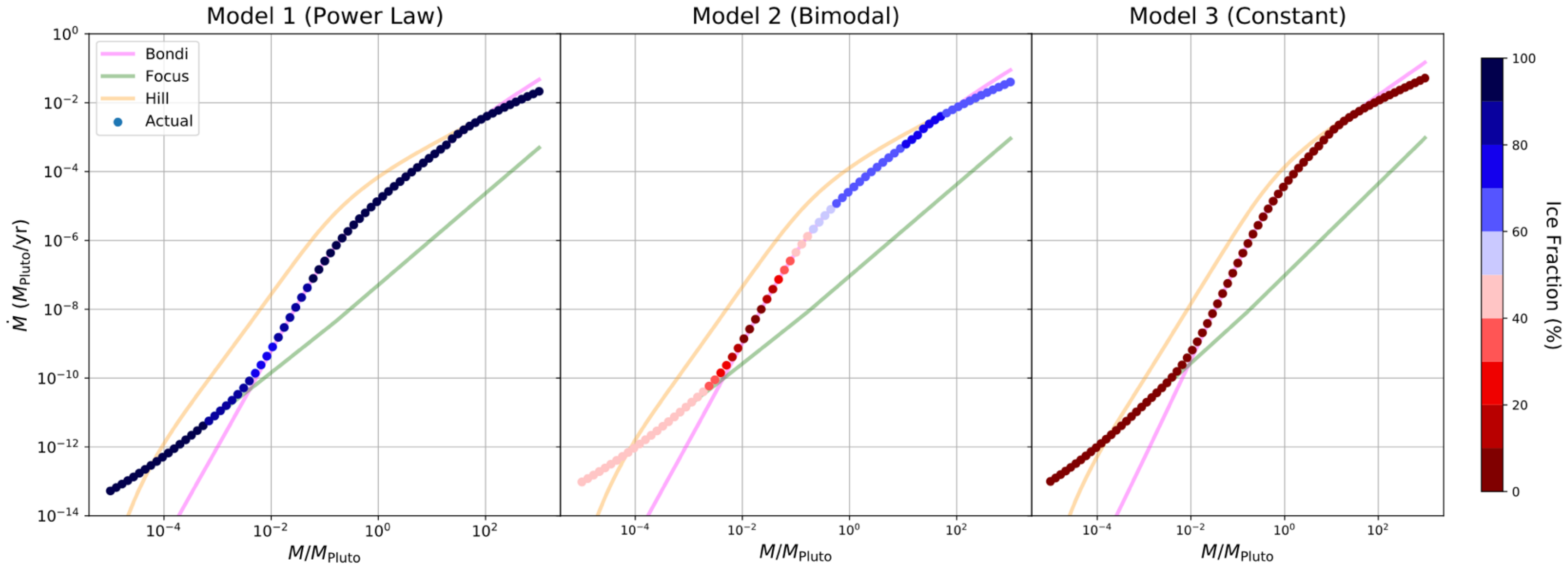

Canas+Lyra et al. 2024

The gap through history…

Brown 2013

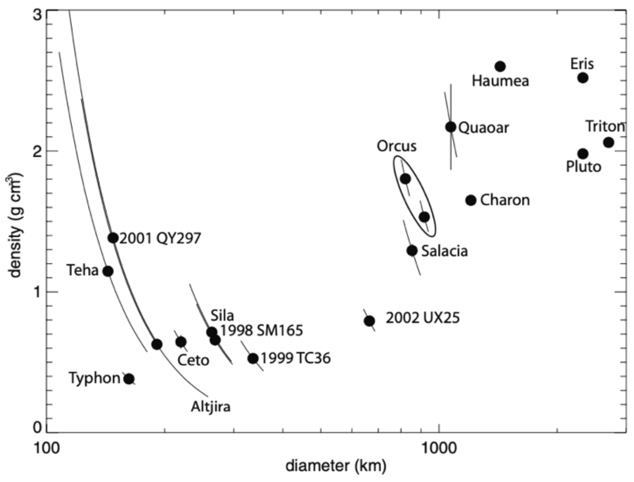

Grundy et al. 2015

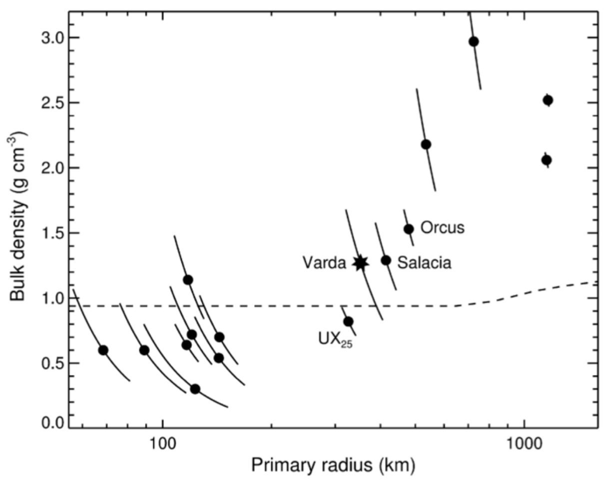

McKinnon et al. 2017

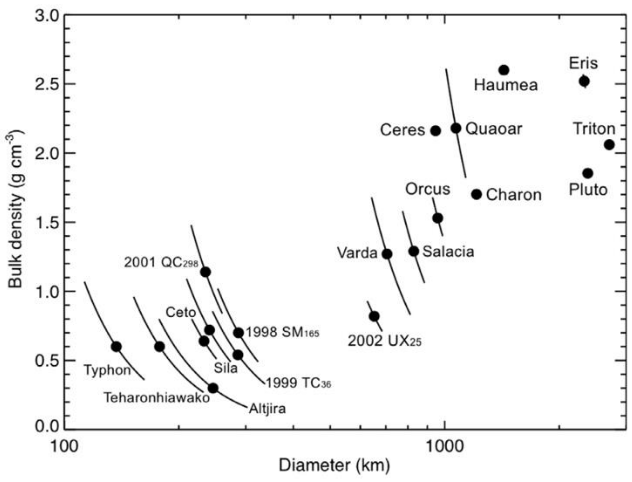

Bierson & Nimmo 2019

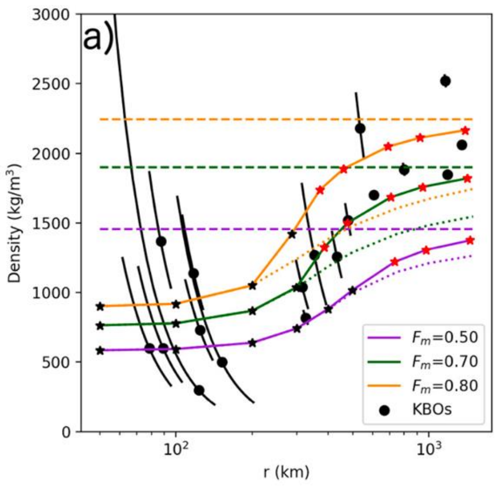

Noll et al. 2020

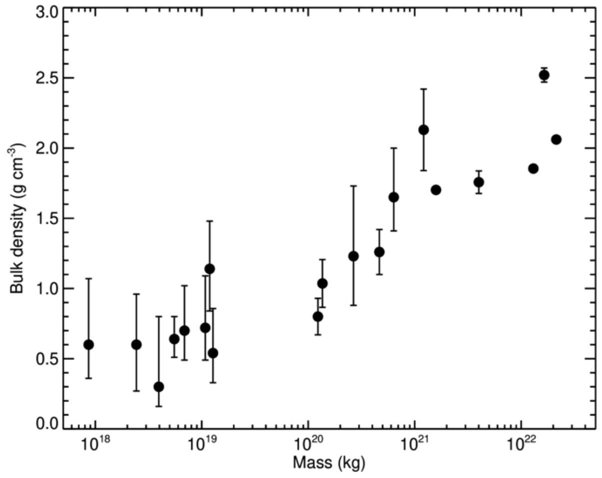

Canas et al. 2024

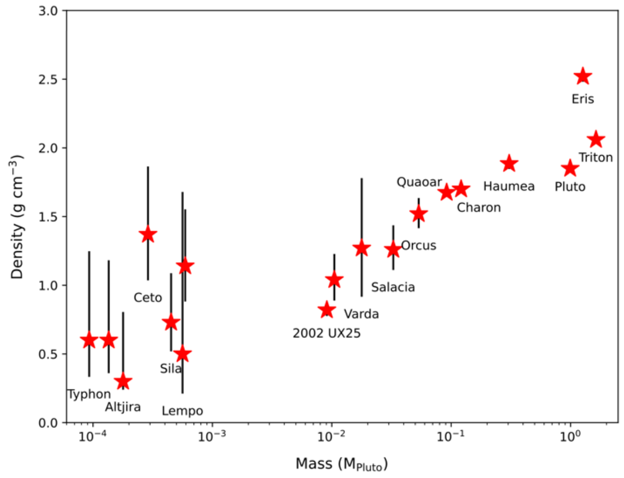

Rommel et al. 2025

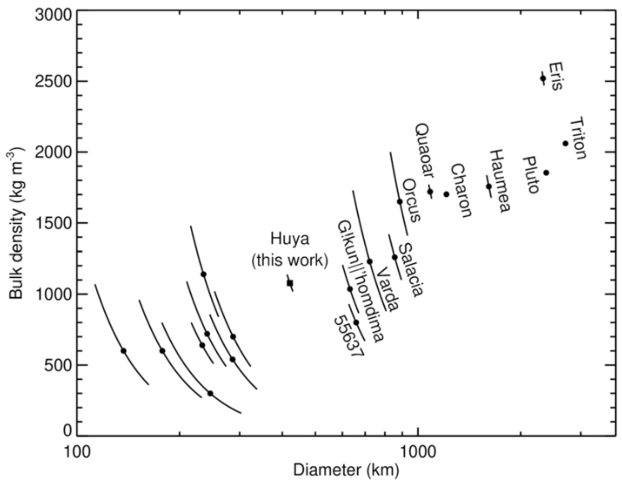

Kozai + Tidal Friction + Drag

$$\frac{de}{dt} = -e\left[V_1 + V_2 + V_d + 5\left(1-e^2\right)S_{eq}\right],$$
$$\frac{dh}{dt} = -h\left(W_1 + W_2 + W_d - 5e^2 S_{eq}\right),$$
$$\frac{d\hat{e}}{dt} = \left[Z_1 + Z_2 + \left(1-e^2\right)\left(4S_{ee} - S_{qq}\right)\right]\hat{q} - \left[Y_1 + Y_2 + \left(1-e^2\right)S_{qh}\right]\hat{h},$$
$$\frac{d\hat{h}}{dt} = \left[Y_1 + Y_2 + \left(1-e^2\right)S_{qh}\right]\hat{e} - \left[X_1 + X_2 + \left(4e^2+1\right)S_{eh}\right]\hat{q},$$
$$\frac{d\mathbf{\Omega}_1}{dt} = \frac{\mu_r h}{I_1}\left(-Y_1\hat{e} + X_1\hat{q} + W_1\hat{h}\right),$$
$$\frac{d\mathbf{\Omega}_2}{dt} = \frac{\mu_r h}{I_2}\left(-Y_2\hat{e} + X_2\hat{q} + W_2\hat{h}\right).$$

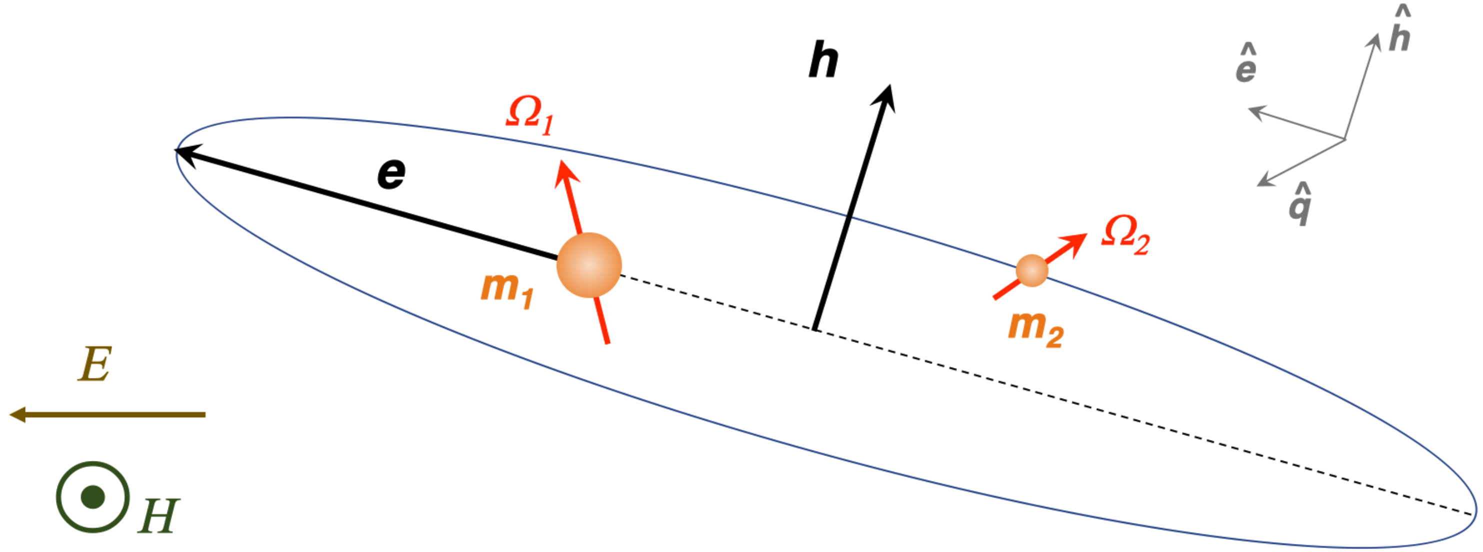

Lyra et al. (2021)

Drag time in McKinnon et al. *1-2 Myr* vs Lyra et al. *10-20 Myr*

Traced to four different assumptions:

1) Disk model (density and temperature)
2) Viscosity
3) Drag coefficient
4) Drag time

Quantity	McKinnon et al. (2020)	Lyra, Youdin, & Johansen (2021)	Factor	Impact on τ_{drag}
Density	10^{-10} kg/m^3 (Desch et al.)	3×10^{-11} kg/m^3 (MMSN)	**1.15**	23 Myr -> 20 Myr
Temperature	30K	42K		
Kinematic viscosity	7×10^4 m^2/s (used sound speed)	1.4×10^5 m^2/s (used mean thermal velocity)	**1.8**	20 Myr -> 13 Myr
Drag coefficient C_d	$24/\mathrm{Re}^{0.6}$	$24/\mathrm{Re}(1+0.27)^{0.43} + 0.47[1-\exp(-0.04\mathrm{Re}^{0.38})]$	**1.5**	13 Myr -> 9 Myr
Drag time τ_{drag}	$\rho R/(C_d \rho_g u_{wind})$	$8/3 \times \rho R/(C_d \rho_g u_{wind})$	**2.7**	9 Myr -> 3 Myr

W. Lyra

The Astrophysical Journal, 733:56 (9pp), 2011 May 20 doi:10.1088/0004-637X/733/1/56

WIND-SHEARING IN GASEOUS PROTOPLANETARY DISKS AND THE EVOLUTION OF BINARY PLANETESIMALS

Hagai B. Perets and Ruth A. Murray-Clay
Harvard-Smithsonian Center for Astrophysics, 60 Garden Street Cambridge, MA 02338, USA
Received 2010 December 13; accepted 2011 March 18; published 2011 May 4

3.2.1. Linear Drag Regime

In the following treatment, we assume that $v_{\rm bin}$ remains constant over a single binary orbital period $P_{\rm bin}$, which is good for $v_{\rm bin}/\dot{v}_{\rm bin} \gg P_{\rm bin}$. Note that this assumption requires not only that $\tau_{\rm merge} \gg P_{\rm bin}/2$ but also that $m_s v_{\rm bin}/F_{D,{\rm disk}} \gg P_{\rm bin}$, where $F_{D,{\rm disk}}$ is the drag force experienced by the small body moving at relative velocity $v_{\rm disk}$ with respect to the gas. We address the complication of non-circular orbits in future work.

In the linear regime, $F_D \propto v_{\rm rel}$, with $v_{\rm rel}$ equal to the relative velocity of the small body with respect to the gas, containing components from the binary orbit and from the overall motion of the binary through the gas disk. Therefore, $F_{D,1} \equiv F_D/v_{\rm rel}$ is constant over the binary orbit. The linear regime is valid for the Epstein and Stokes drag regimes, but the value of $F_{D,1}$ in the two regimes differs (see Section 2.1). We may now express the orbit-averaged drag force as

$$\langle F_D \rangle = \frac{1}{2\pi}\int_0^{2\pi} F_D\, d\theta$$
$$= \frac{F_{D,1}}{2\pi}\int_0^{2\pi} (v_{\rm bin}\sin\theta + v_{\rm disk})\, d\theta = F_{D,1} v_{\rm bin}, \quad (21)$$

wind averages out

where θ is the angle of the binary in its orbit. The term $v_{\rm bin}\sin\theta$ is the bulk velocity component of the small planetesimal parallel to the direction of motion in the binary frame of reference, so that $v_{\rm rel} = v_{\rm bin}\sin\theta + v_{\rm disk}$. Over a full orbit the contribution from $v_{\rm disk}$ averages out and

$$\tau_{\rm merge} = \frac{t_{\rm stop}}{2}\,, \quad (22)$$

with $t_{\rm stop}$ equal to the stopping time of a single small planetesimal in the gaseous protoplanetary disk:

$$t_{\rm stop} = \frac{m_s}{F_{D,1}} = \begin{cases} \left(\frac{\rho_p}{\rho_g}\right)\frac{r_s}{\bar{v}_{\rm th}} & \text{Epstein} \\ \frac{4}{9}\left(\frac{\rho_p}{\rho_g}\right)\frac{r_s^2}{\lambda\bar{v}_{\rm th}} & \text{Stokes.} \end{cases}$$

Recall that in the linear regime, the stopping time is independent of the relative velocity between the planetesimal and the gas. Note that single planetesimals with stopping times longer than an orbital time inspiral into the star on a timescale of $\sim t_{\rm stop}/\eta$. The same processes are at work in both cases—infall into the star is slower than binary coalescence because the gas and planetesimals orbit the star together, reducing their relative velocities.

The timescale for coalescence is independent of $d_{\rm bin}$, and the total merger time for a binary is

$$T_{\rm merge} = \tau_{\rm merge}\ln\left(\frac{d_0}{r_b}\right)\,, \quad (23)$$

where $d_{\rm bin} = d_0$ initially, and r_b is the final binary separation before coalescence.

3.2.2. Quadratic (Ram Pressure) Regime

We now consider the quadratic regime, for which $F_D \propto v_{\rm rel}^2$, appropriate for ram pressure drag. Following the same procedure as above, but using $F_{D,2} \equiv F_D/v_{\rm rel}^2$ with $F_{D,2}$ a constant, we get

$$\langle F_D \rangle = \frac{F_{D,2}}{2\pi}\int_0^{2\pi}(v_{\rm bin}\sin\theta + v_{\rm disk})^2 d\theta$$
$$= F_{D,2}v_{\rm bin}^2\left[1 + \frac{1}{2}\left(\frac{v_{\rm disk}}{v_{\rm bin}}\right)^2\right]. \quad (24)$$

wind doesn't average out

In other words, the ram pressure drag force requires an effective relative velocity correction of $[1+0.5(v_{\rm disk}/v_{\rm bin})^2]$—in this case the contribution from the bulk velocity drag did not average out.

Now,

$$\tau_{\rm merge} = \frac{t_{\rm stop}(v_{\rm bin})/2}{1+0.5(v_{\rm disk}/v_{\rm bin})^2}\,, \quad (25)$$

where $t_{\rm stop}(v_{\rm bin})$ is the stopping time for $v_{\rm rel} = v_{\rm bin}$. In the quadratic regime, $t_{\rm stop}$ is not independent of $v_{\rm rel}$, so to make dependences clearer, we rewrite this expression as

$$\tau_{\rm merge} = \frac{m_s/(2F_{D,2})}{v_{\rm bin}[1+0.5(v_{\rm disk}/v_{\rm bin})^2]} \approx \begin{cases} \frac{m_s}{2F_{D,2}v_{\rm bin}}, & v_{\rm bin} \gg v_{\rm disk} \\ \frac{m_s v_{\rm bin}}{F_{D,2}v_{\rm disk}^2}, & v_{\rm bin} \ll v_{\rm disk} \end{cases}. \quad (26)$$

Plugging in $F_{D,2}$ for ram pressure drag and $v_{\rm bin} = (Gm_b/d_{\rm bin})^{1/2}$, this corresponds to

$$\tau_{\rm merge} \approx \frac{2}{0.66}\left(\frac{\rho_p}{\rho_g}\right) r_s \times \begin{cases} d_{\rm bin}^{1/2}/\sqrt{Gm_b}, & v_{\rm bin} \gg v_{\rm disk} \\ 2\sqrt{Gm_b}/(d_{\rm bin}^{1/2}v_{\rm disk}^2), & v_{\rm bin} \ll v_{\rm disk} \end{cases}. \quad (27)$$

W. Lyra

Perets & Murray-Clay (2011)

Linear vs quadratic drag

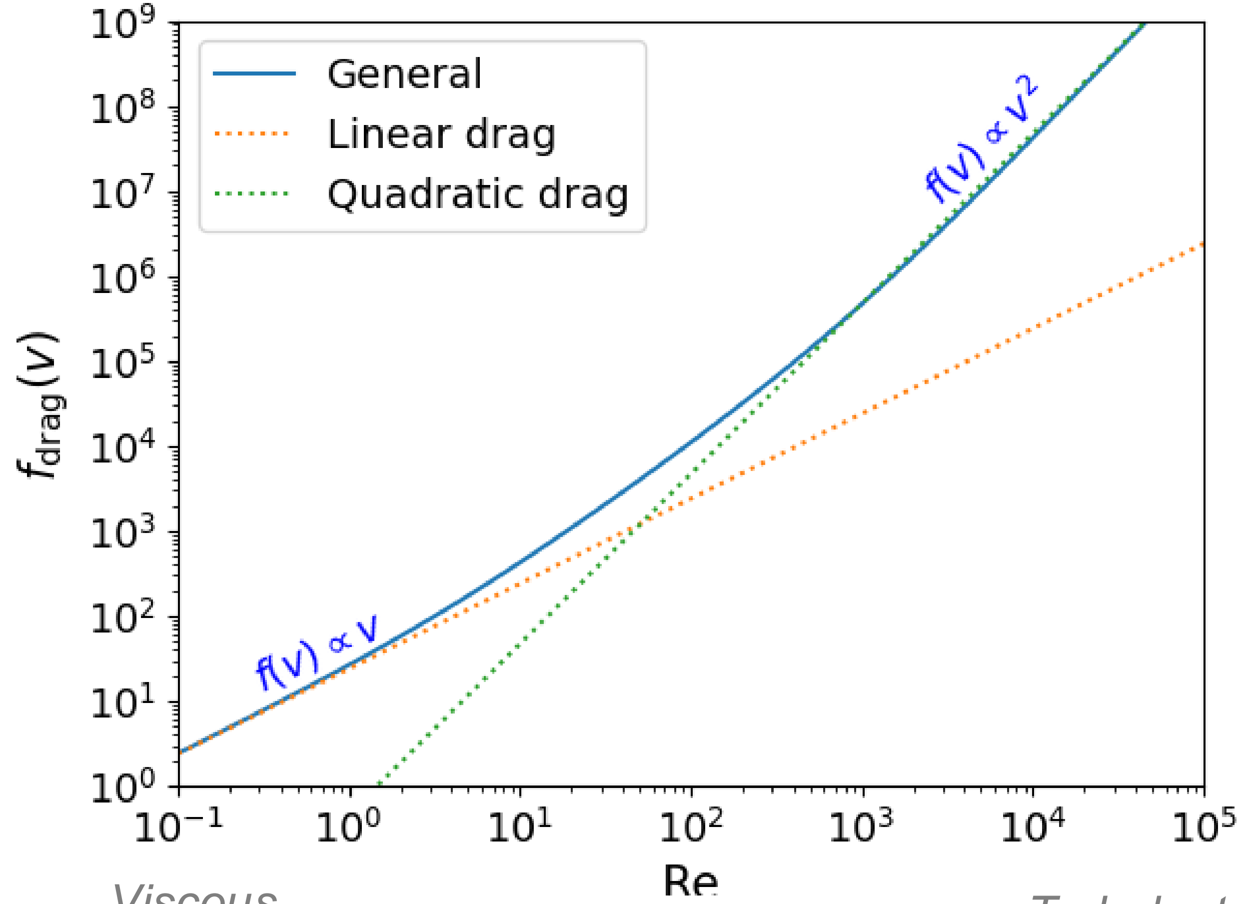

Viscous *Turbulent*

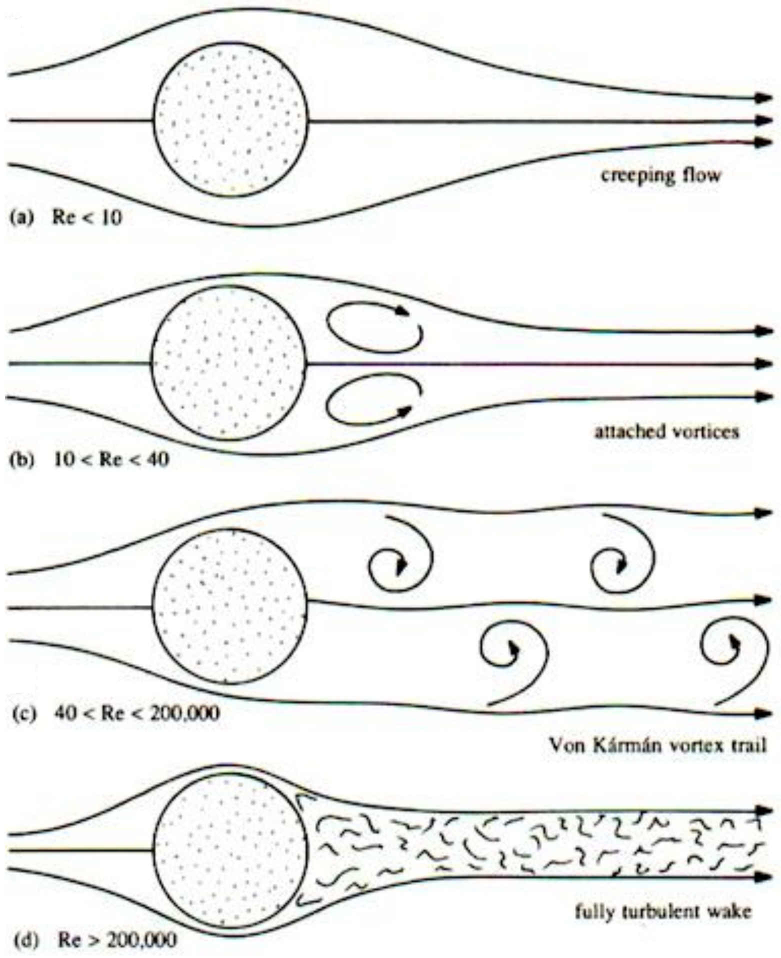

Reynolds number

W. Lyra

Lyra et al. (2021)